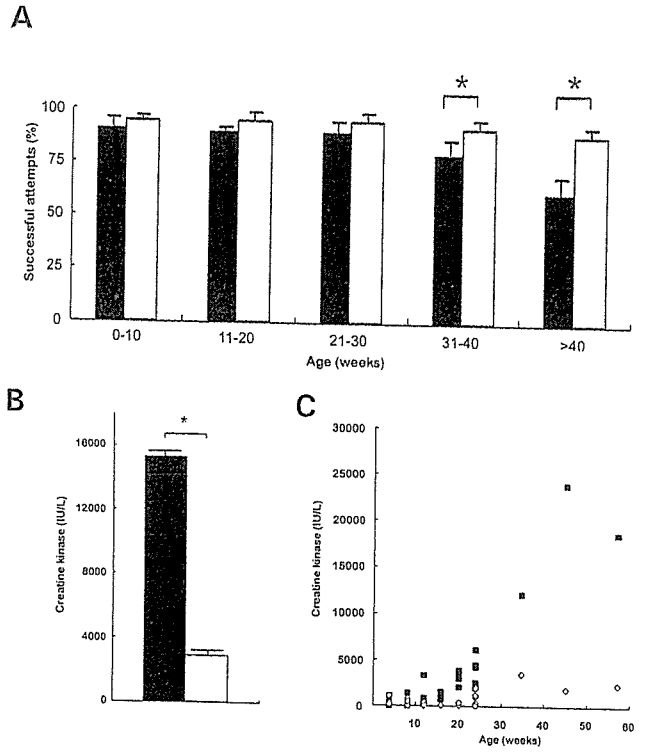

Figure 5. (A) Evaluation of over-all motor strength using rod-climbing test, according to age group. Mean of three trials are shown. $Gne^{(-/-)}$ h*GNE*V572L-Tg mice (closed bars, $n = 10$) perform worse than littermates ($n = 10$). Significant difference is noticeable after 30 weeks of age. Asterisk, $P < 0.05$ (Mann–Whitney U test). (B) Measurement of CK activity. Serum CK is significantly higher in $Gne^{(-/-)}$h*GNE*V572L-Tg mice (closed bars) when compared with littermates (open bars). Asterisk, $P < 0.05$ (Student's t-test, two-tailed). (C) CK activity according to age. CK activity of $Gne^{(-/-)}$ h*GNE*V572L-Tg mice (closed squares) starts to elevate after 30 weeks of age when compared with littermates (open diamonds).

Various proteins are expressed in the $Gne^{(-/-)}$h*GNE*V572L-Tg muscles

One of the defining hallmark features of DMRV/h-IBM is the presence of inclusion bodies that are presumed to have a role in muscle degeneration. These deposits have been shown to be immunoreactive to several proteins. Similar to human cases of DMRV, muscle cross sections obtained from the $Gne^{(-/-)}$ h*GNE*V572L-Tg mice reveal positive Congo red staining (Fig. 7D), which is not observed in the myofibers of control mice (data not shown). Intense, demarcated signals are seen within the area of RVs and more frequently co-localizing with inclusion bodies which are often seen in DMRV/h-IBM. As congophilia denotes deposition of proteins assuming a beta-pleated structure, we used the well-characterized 6E10, Aβ1–42, Aβ1–40 and A11 (amyloid β-oligomer), and β-site amyloid precursor protein cleaving enzyme (BACE2) antibodies to check for intracellular accumulation of amyloid. Amyloid depositions occur within the myofibers, and are seen to be occasionally associated with vacuolated fibers, as ~62% of RVs are positive for amyloid expression (data not shown). These amyloid inclusions are also noted in non-vacuolated fibers, including those which appear normal. Amyloid β precursor protein (AβPP), which is recognized by 6E10 antibody (Fig. 7I) has intense, large, fairly demarcated immunoreactive signals within the RVs, similar to the staining pattern of the fibrillar forms of amyloid β or amyloid β peptides 1–42 and 1–40 (Fig. 7J and K). In good agreement with finding amyloid deposits in the myofibers, BACE2, which purportedly represents β-secretase activity, is upregulated in these myofibers and are seen as granular staining in the cytoplasm and intense immunoreactivity at subsarcolemmal areas (Fig. 7H). Interestingly, the oligomer form of amyloid β, which is recognized by A11, is also expressed in the myofibers; positive signals are seen as aggregates around the RVs which are localized in areas distinct from fibrillar forms of amyloid (Fig. 7L).

We then analyzed skeletal muscles of mice from different age groups to see whether these amyloid accumulations are related to or can be considered as a function of age. We found out that these accumulations start to occur from 32 to 34 weeks of age, a period when virtually no RV is seen in the myofibers, and muscle pathology is characterized mainly by mild variation in fiber size (Fig. 8A and C). Both AβPP (Fig. 8B) and amyloid β 1–42 peptide (Fig. 8D) show positive immunoreactivity within the myofibers.

The microtubule-associated protein tau, a cytoskeletal protein, has been shown to be abnormally phosphorylated and accumulated in DMRV and other muscle disorders (21–23). Similarly, in these mice, these deposits are evident as squiggly inclusions which are occasionally seen in vacuolated fibers (Fig. 7M).

SM-31, an antibody which detects neurofilaments, has been well-characterized in DMRV/h-IBM (21,24). In muscle sections, positive staining is seen within the vicinity of RVs (Fig. 7N); not all RVs, however, show immunoreactivity with this antibody. SM-310, on the other hand, only stains the intramuscular nerve bundles (Fig. 7O).

Because of the accumulation of several proteins in the myofibers, ER stress and the unfolded protein response (UPR) have been implicated in the pathogenesis of DMRV/h-IBM. Using an antibody which recognizes one of the ER chaperones, we show that the UPR activation occurs in the $Gne^{(-/-)}$ h*GNE*V572L-Tg mice. Intracellular Grp-94 immunoreactivity is seen exclusively in vacuolated fibers (Fig. 7P). In the myofibers of the mice, strong reactivity to ubiquitin antibody in vacuolated and non-vacuolated fibers are seen (Fig. 7Q), suggesting that the ubiquitin–proteosome system may as well be involved in the degradation of abnormal protein accumulations in the muscle, and that misfolded proteins are ubiquitinated but not degraded.

Sarcolemmal proteins are also accumulated in DMRV/h-IBM myofibers. Within the vicinity of the RVs, positive α-dystroglycan (Fig. 7R), β-dystroglycan (Fig. 7S) and α-sarcoglycan (Fig. 7T) signals are observed.

In the myofibers of the control mice, no protein depositions were appreciated (data not shown).

Electron microscopic studies show evidence of autophagy and inclusions in the $Gne^{(-/-)}$h*GNE*V572L-Tg muscles

Ultrastructural studies confirm the activation of autophagy in $Gne^{(-/-)}$h*GNE*V572L-Tg muscles (Fig. 9). We obtained samples from a 42-week-old female mouse which had RVs

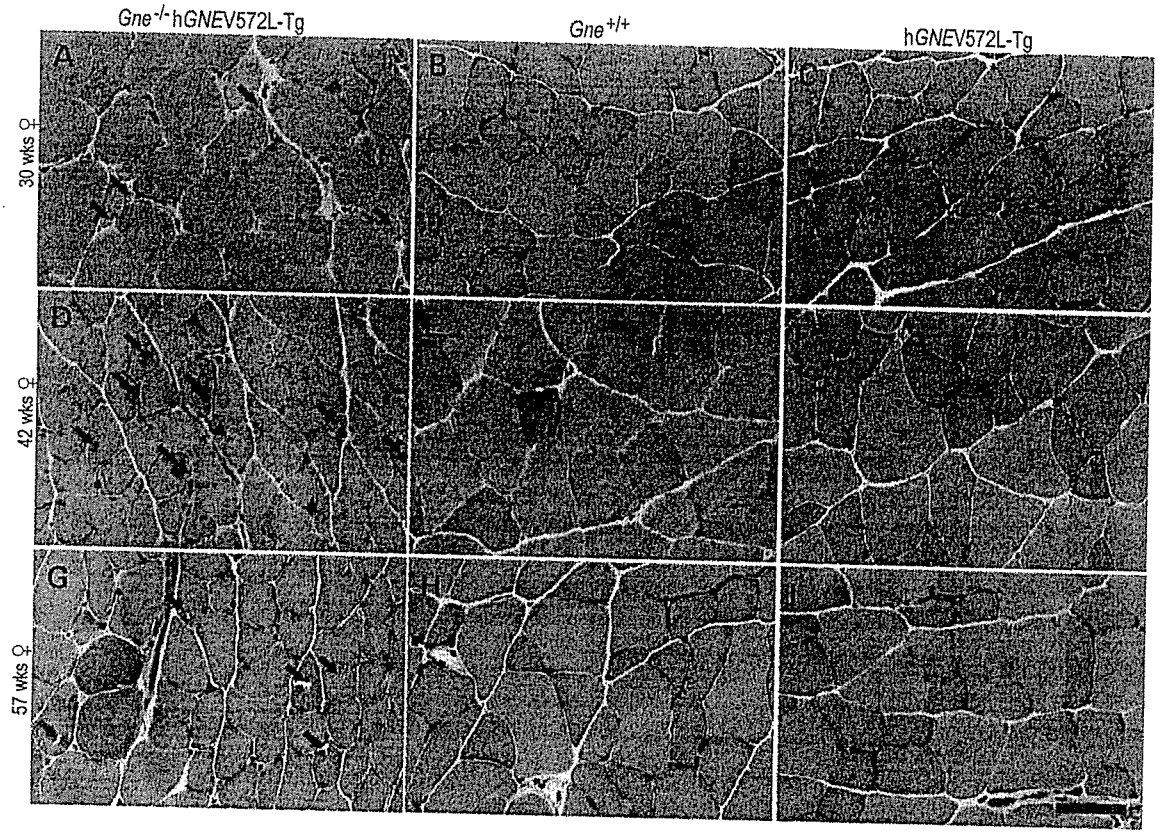

Figure 6. Hematoxylin and eosin sections from $Gne^{(-/-)}$h*GNE*V572L-Tg (**A, D, G**), WT (**B, E, H**), h*GNE*V572L-Tg (**C, F, I**). The h*GNE*V572L-Tg mice are comparable with WT in all ages. In the $Gne^{(-/-)}$h*GNE*V572L-Tg, there is variation in fiber size which becomes more obvious as the mice age. Fibrosis, necrotic or regenerating processes are not noted. Internalized nuclei are noted in scattered fibers. Small angular fibers are noted from around 30 weeks of age (A, arrows). Fibers with RVs (arrows), as well as cytoplasmic inclusions (arrowhead) are observed in scattered fibers from 42 weeks of age (D and G). Bar represents 40 μm.

as seen in light microscopy. In these samples, disorganization of myofibrils was seen in the vicinity of RVs. In about 500 myofibers examined, 10% showed ultrastructural evidence of autophagy. Collections of lysosomal autophagosomes containing undigested intracellular debris were seen, usually enclosed by a limiting membrane (Fig. 9A, arrow). The debris are often composed of light or electron-dense amorphous materials, and appeared like myelin whorls. Multiple small double membrane-bound autophagic vacuoles were often contained within a larger autophagic vesicle (AV), suggesting that autophagy in these myofibers involves a continual process of AV consolidation (Fig. 9A, arrowhead). Multilamellar bodies are also observed (Fig. 9A, double arrows). Probable amyloid deposits are seen as amorphous and granular material (Fig. 9B, magnified from A). Interestingly, ovoid and densely granular deposits, which may also be amyloid-like structures, are noted not only in the areas of autophagy (Fig. 9A, asterisk), but also in areas where myofibrillar architecture is well preserved (Fig. 9C). Occasionally, autophagic vacuoles are seen within the substance of these deposits (Fig. 9C, arrow).

$Gne^{(-/-)}$h*GNE*V572L-Tg shows pathological changes in the diaphragm and cardiac muscles

It has been a well-accepted fact that DMRV/h-IBM primarily involved the skeletal muscles, and that respiratory muscles are assumed to be spared as there had been no reports implying the involvement of the respiratory system. Interestingly, in the $Gne^{(-/-)}$h*GNE*V572L-Tg mice, we found that even diaphragm muscles are involved, although the findings range from almost normal findings to the presence of marked fibrosis and RVs in the myofibers (Fig. 10A). Likewise, we have observed inclusion bodies which are seen in both vacuolated and non-vacuolated fibers (data not shown).

It is now being recognized that some patients manifest with a variety of cardiac abnormalities, from the seemingly benign right bundle branch block to fatal arrhythmias. This led us to carefully check the status of cardiac muscles in the mice. We found out that few mice (around 20%) develop fibrosis in the cardiac tissue after the age of 30 weeks, and some show marked endomysial fibrosis (Fig. 10B). Moreover, amyloid deposition (Fig. 10C) and, occasionally, RVs (Fig. 10D) are also observed in cardiomyocytes. We also tried to functionally evaluate the heart using 2D echocardiography and electrocardiogram, but we did not observe any abnormality pointing to definite cardiomyopathy or conduction defects (data not shown), although we only tested a limited number of mice.

DISCUSSION

Sialylation of oligosaccharide chains is a common and physiologically important event, and sialic acids are probably the

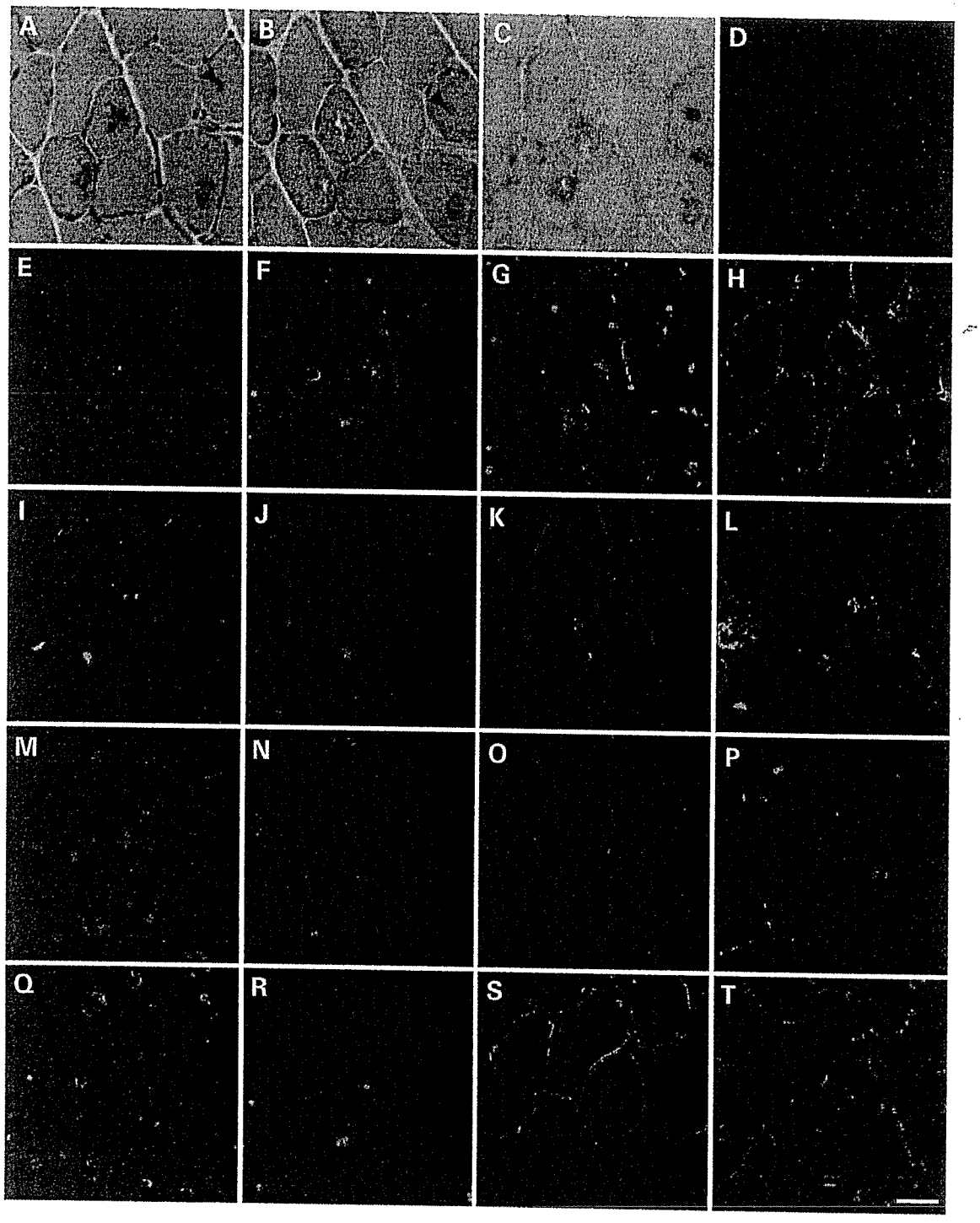

Figure 7. Serial sections taken from a 42-week-old female *Gne*$^{(-/-)}$h*GNE*V572L-Tg mouse. (**A**) Hematoxylin and eosin sections show fibers with RVs and cytoplasmic inclusions. (**B**) In modified Gomori trichrome, vacuoles are rimmed by eosinophilic granules. (**C**) Acid phosphatase activity is enhanced around RVs, suggesting upregulation of lysosomal activity in these areas. (**D**) Congo red staining visualized by Texas red filters shows positive staining in fibers with or without RVs, and appear as large, granular deposits. Immunoreactivity to lysosomal proteins confirm the presence of autophagy in fibers with RVs: (**E**) LAMP-1 signals are seen in the areas of RVs; (**F**) LAMP-2 has subsarcolemmal immunoreactivity, in addition to positive staining in RVs; (**G**) LC3 stains the same areas as LAMP-2, in addition to the perinuclear areas. Intracellular deposition of amyloid is seen in vacuolated or non-vacuolated fibers: (**H**) Increased reactivity to BACE2 is seen in the cytoplasm of fibers with RVs and within the vicinity of RVs; (**I**) AβPP expression is intense in area of RVs, seen as discrete deposits; (**J**) amyloid β 1–42 and (**K**) amyloid β 1–40 stainings are likewise seen as discrete deposits within the vicinity of RVs; (**L**) amyloid β-oligomeric antibody signals are noted as aggregates of small granule-like deposits around the RVs. Neurofilament deposition is observed in the myofibers: SM-31 (**M**) immunoreactivity is occasionally noted within the vicinity of RVs, whereas SM-310 (**N**) only stains intramuscular nerve bundles. (**O**) Epitopes of phosphorylated tau are observed in some fibers with RVs. (**P**) Fibers with RVs have intense ubiquitin staining around RVs and granule-like signals in these fibers. (**Q**) Grp94, an endoplastic reticulum luminal stress protein, is upregulated exclusively in vacuolated fibers as large granular deposits within the RVs. Sarcolemmal proteins are deposited within the vicinity of RVs: (**R**) α-dystroglycan; (**S**) β-dystroglycan; and (**T**) α-sarcoglycan. Bar represents 20 μm.

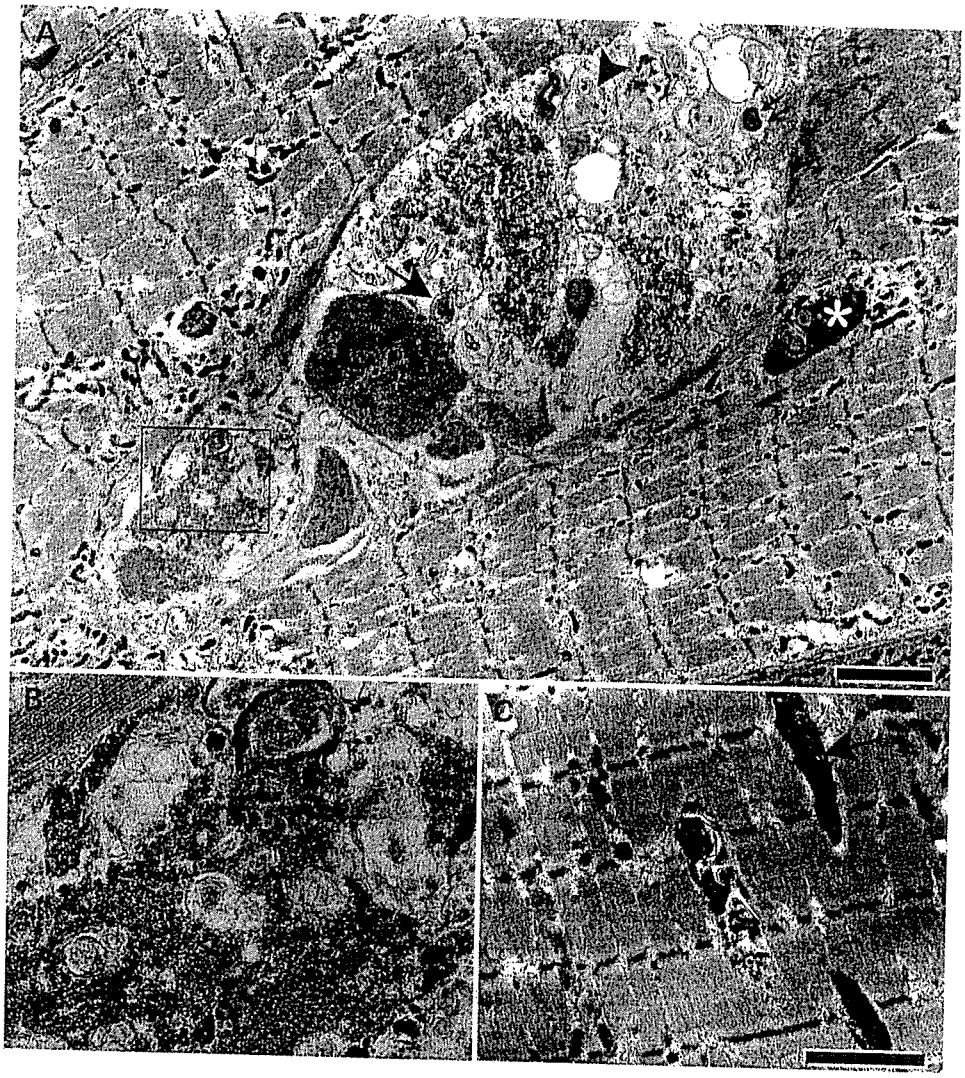

Figure 8. Ultrastructural evidence of autophagy and intracellular inclusions. (**A**) Collections of lysosomal autophagosomes with intracellular debris which are light or electron-dense amorphous materials enclosed by a limiting membrane (arrow). Multilammelar structures are also observed (double arrows). Ovoid and dense deposits which are probably amyloid deposits are likewise seen (asterisk) (**B**) Probable amyloid deposits are seen as amorphous and granular material surrounded by autophagosomes (B, magnified from A). (**C**) Dense, granular deposits which are probably amyloid accumulations are also noted in areas where architecture of myofibrils are generally well preserved; occasionally, autophagic vacuoles are seen within the substance of these deposits (arrow). Bar represents 2 μm.

most biologically important monosaccharide units of glycoconjugates. These negatively charged sugars at the terminal ends of glycoconjugates have very important biological roles in mammalian development, and this is underscored by the embryonic lethality resulting from attempts to knock-out *Gne* in the mice (20), and further supported by the absence of homozygous null mutations in humans. Making a transgenic *GNE* mouse on a *Gne* knockout background thus allowed us to rescue the phenotype in *Gne* knockout. Clearly, the $Gne^{(-/-)}$h*GNE*V572L-Tg resembles the phenotype in human DMRV/h-IBM patients.

It is conceivable that a mutation in the *GNE*, a gene responsible for catalyzing the rate-limiting step in sialic acid biosynthesis, can lead to hyposialylation. Most, if not all, of the mutations causing DMRV caused partial reduction of the enzymatic activity of either UDP-GlcNAc 2-epimerase or ManNAc kinase of the GNE (17,19). As we have predicted, our results show that there is a marked reduction in sialic acid level, which can reflect the enzymatic activity of GNE, in the serum and other tissues of the $Gne^{(-/-)}$h*GNE*V572L-Tg mice. With regards to the expression of *GNE* in various tissues, it has been shown that expression in the muscle is very low (25). Our results show, on the other hand, that mRNA expression of h*GNE*V572L-Tg is highest in the muscle, and we attribute this to the promoter that we used in the transgene construct. Previously, we have shown that CAG promoter efficiently promotes expression of a gene into adult skeletal muscles (26).

Skeletal muscle is mainly affected in DMRV/h-IBM, although it is reasonable to expect multi-organ involvement because of the ubiquitous expression of *GNE*. In our mice, the skeletal muscle is clearly affected despite the data that

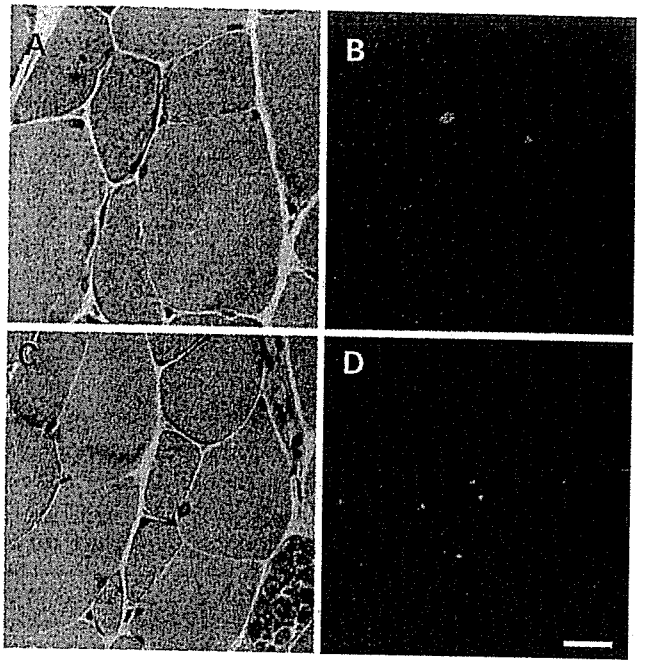

Figure 9. Amyloid deposition precedes RV formation. Sections taken from the gastrocnemius of a 34-week-old female mouse shows variation in fiber size in hematoxylin and eosin sections (**A** and **C**). Note the absence of RVs or cytoplamic inclusions in these fibers. Amyloid depositions are seen as immunofluorescent signals in small fibers (**B**, amyloid β 1–42; **D**, AβPP). Bar represents 20 μm.

hyposialylation is not that remarkable when compared with other organs. Our results suggest that even a slight reduction in sialic acid level can cause symptoms in skeletal muscles; however, the selectivity of skeletal muscle may not be explained by the *Gne* expression levels and sialic acid levels in each organ.

It is notable that some of the $Gne^{(-/-)}$h*GNE*V572L-Tg mice die sooner than their littermates, but the precise reason for this is not known at present. It is, however, evident that a significant number of the autopsied mice showed pathological findings in the diaphragm and the heart. In humans, there was a report on two siblings with the homozygous V572L mutation who died from arrhythmia (27), but there had been no reports on respiratory involvement among patients.

The onset of symptoms among DMRV patients has been reported to be from the second to the third decade (3), although there were anecdotal reports of earlier onset (28). Interestingly, in the $Gne^{(-/-)}$h*GNE*V572L-Tg mice, the onset of clinical phenotype is noted around 30 weeks of age, which can be considered to be similar to that in humans, using lifespan and ability to reproduce for points of comparison. It is peculiar that gastrocnemius and quadriceps muscles are preferentially involved in mice, while in humans, the tibialis anterior is remarkably involved while the quadriceps are affected relatively late in the course of the disease. In our recent data on the clinical presentation of DMRV, however, it is clear that the gastrocnemius can be affected more severely in some cases (28).

We tried to check fiber type involvement in these muscles, and found out that both slow and fast fibers are affected in human and mice, in terms of the presence of RVs, but fast type fibers are predominantly involved (data not shown). Sporadic IBM has some pathological similarities with DMRV; recently, it has been shown that the presence of inclusions on routine histochemistry and the pathogenic accumulation of β-amyloid protein occur in fast twitch muscles, both in a transgenic model of IBM and in IBM patients (29), implying that fast type fibers are more vulnerable to pathological changes. Further analysis is needed on this aspect to derive a more conclusive data.

CK levels are reported to be mildly or moderately elevated in patients, although there were isolated cases where the CK activity was above 1000 IU/L (11). CK elevation has always been correlated with the presence of necrotic and regenerating processes in the skeletal muscle, but which are only occasionally found in DMRV/h-IBM. Elevation of serum CK is also seen in the $Gne^{(-/-)}$h*GNE*V572L-Tg mice, although necrotic and regenerating process is barely detectable. Our data suggest that there might be other mechanisms which trigger CK release into the circulation, aside from myonecrosis. It has not been clarified if CK release into the blood stream may be induced by deglycosylation of membrane proteins, although some studies suggested that removal of sialic acids by neuraminidase treatment may influence sarcolemmal permeability (30). Further tests are clearly needed to shed some insight on the CK elevation in DMRV/h-IBM and $Gne^{(-/-)}$ h*GNE*V572L-Tg mice.

A subject of poignant interest is whether RV formation, one of the hallmarks of DMRV/h-IBM, is the primary event that induces muscle fiber atrophy and loss, notwithstanding the fact that RVs are non-specific and could be seen in a multitude of myopathies. In the $Gne^{(-/-)}$h*GNE*V572L-Tg mice, weakness is clearly noted before the occurrence of RVs, implying that other factors should be responsible for the earlier onset of weakness. Consistently, we have documented that serum and other tissues are hyposialylated, and this phenomenon is not at all correlated with age, strongly suggesting that hyposialylation may play a role in the development of clinical manifestations exhibited by patients. Previous studies have implicated that sialic acid directly contributes to the negative surface potential of cells, because desialylation of rat skeletal muscle sodium channel leads to reduced sensitivity of these channels to the effects of external calcium (31). This would mean that voltage gating parameters are shifted to the point that channels required a larger depolarization in order to gate, which may suggest that the mechanism of weakness may be due to the reduced excitability of the muscle membrane as a result of sodium channel desialylation.

The hallmarks of DMRV/h-IBM include RVs that are autophagic in nature (32) and cytoplasmic inclusions in vacuolated and non-vacuolated fibers, both of which are seen in muscle sections from the $Gne^{(-/-)}$h*GNE*V572L-Tg mice. Several proteins have been shown to accumulate in DMRV myofibers (33,34), and most of which have been demonstrated to be mainly associated with amyloid because of the positive reactivity to crystal violet and Congo red, suggesting that they assume the beta-pleated sheet configuration. In general, more than 20 unrelated proteins, including β-amyloid (34), prion, tau (21) and transthyretin, can abnormally unfold and self-aggregate to form beta-pleated sheet amyloid (35). The association of these proteins with DMRV/h-IBM

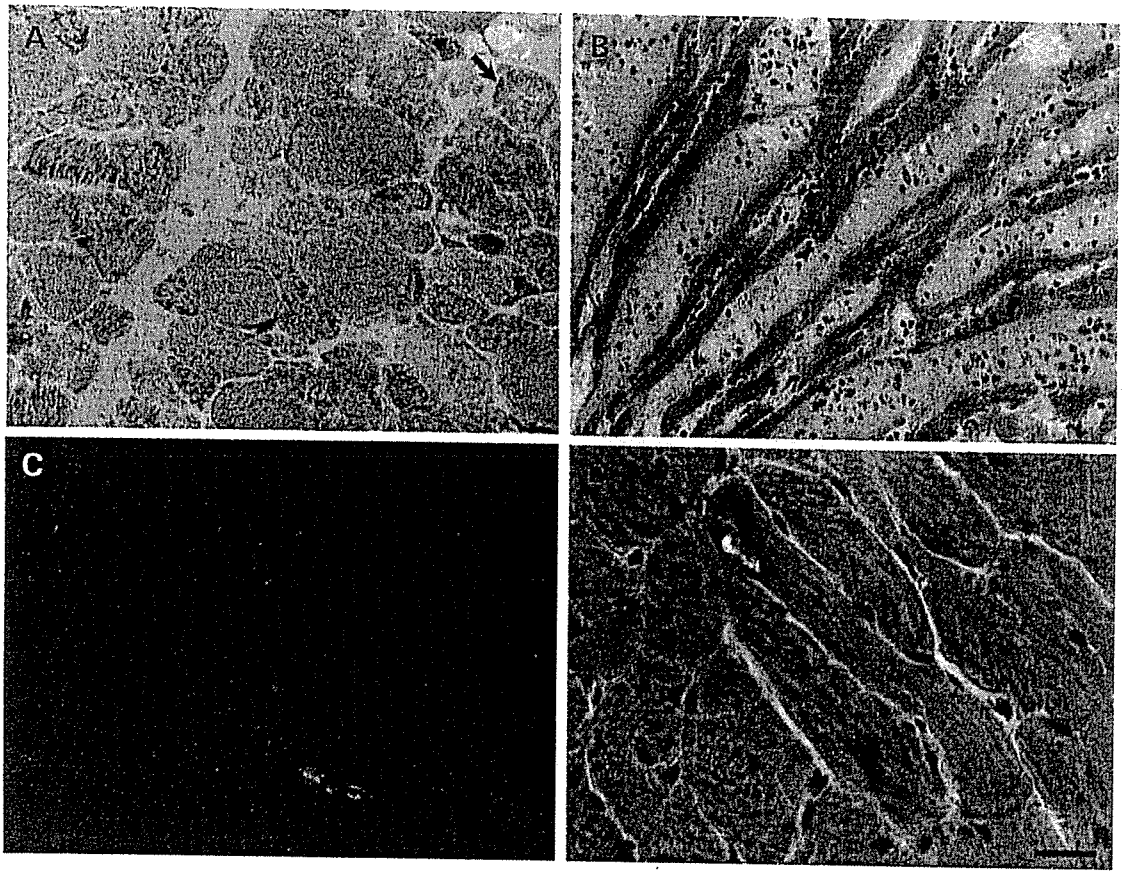

Figure 10. The diaphragm and cardiac muscles are likewise involved in the $Gne^{(-/-)}$h*GNE*V572L-Tg mice. (**A**) Modified Gomori trichrome section of a 48-week-old male $Gne^{(-/-)}$h*GNE*V572L-Tg. Note the presence of endomysial fibrosis and fiber with RV. (**B**) Hematoxylin and eosin sections from a 54-week-old female $Gne^{(-/-)}$h*GNE*V572L-Tg showing marked fibrosis. (**C**) Amyloid deposition (Amyloid β 1–42) is seen in the cardiomyocytes of the same mouse in (B). (**D**) HE section of cardiac muscle from a 42-week-old male $Gne^{(-/-)}$h*GNE*V572L-Tg reveals that RVs are occasionally seen in cardiomyocytes.

pathomechanism has largely been enigmatic up to this time, but unfolding and misfolding of proteins most probably play a role. Previous reports have alluded to the role of sialic acid in proper folding of proteins (35–37). The ultimate fate of aggregated, misfolded glycoproteins is degradation, hence the activation of UPR is expected, which could explain the presence of ubiquitin signals in the myofibers of the $Gne^{(-/-)}$ h*GNE*V572L-Tg mice and upregulation of ubiquitin and proteasome in DMRV/h-IBM myofibers (38).

The implication of amyloid deposition in the formation of RVs in both DMRV/h-IBM and s-IBM (39) is supported by our finding that the occurrence of amyloid inclusions in the myofibers preceded RV formation. Amyloid itself has been shown *in vitro* to block the degradation of ubiquitinated proteins by inhibiting proteasome activity (40), hence its accumulation may not only lead to cytotoxicity, but also may further aggravate protein misfolding. In addition, it has been clarified that overproduction of amyloid can induce tau hyperphosphorylation and decrease its solubility (41). Sialylation and glycosylation of amyloid precursor protein, which contains both *O*- and *N*-glycans, appear to be important for its proteolytic processing, secretion and metabolism (42–45). Interference with the formation of *N*-linked glycans resulted in a decrease in secreted AβPP and an increase in the level of the cellular form of the protein, which has a higher propensity to form amyloid β peptide (42,46). Although amyloid fibrils were the structure previously considered to be cytotoxic, there is current experimental evidence that pre-amyloid oligomeric complexes or aggregates, either diffuse or in a protofibril stage, can be very cytotoxic (47). The presence of dense deposits in areas with relatively preserved myofibrillar architecture on electron microscopy strongly suggest that deposition of amyloid and amyloid-like structures pre-date RV formation.

Because DMRV/h-IBM patients do not present, in general, with symptoms reflecting involvement of the respiratory system, it is assumed that the diaphragm is relatively spared in this myopathy. In the $Gne^{(-/-)}$h*GNE*V572L-Tg mice, it is clear that the diaphragm can be involved, despite the absence of overt respiratory difficulties. The presence of pathological findings in the sacrificed mice, and not only in the ones that died suddenly, may suggest that the presence of RVs *per se*, may not correlate with severity in phenotype, with respect to involvement of diaphragm. A more sensitive method of assessing the respiratory status of these mice, *vis-à-vis* a plain observation, might be helpful in clarifying the extent to which respiratory system is involved. Our results suggest that careful evaluation of respiratory and cardiovascular functions is logical and warranted in human patients.

In the $Gne^{(-/-)}$h*GNE*V572L-Tg mice, we have seen RVs in the cardiac muscles obtained from a couple of mice, clearly supporting the presence of cardiac involvement in DMRV/h-IBM. It has always been reported that DMRV involves primarily skeletal muscles but recently, however, it is being recognized that other organs may likewise be involved. For example, cardiac involvement is not very rare as it is seen in 18% of patients, with a spectrum of manifestations ranging from an incomplete right bundle-branch block to a fatal arrhythmia which led to sudden death (25,26). Sialic acid was shown to be an important component on the surface of heart muscle cells, because its removal reduced the cell surface negative charge by 25% (48) and produced a large increase in cardiac myocyte Ca^{2+}, followed by marked cell contracture (49), emphasizing the importance of negatively charged sialic acid-containing gangliosides in the maintenance of cardiac cell physiological Ca^{2+} permeability. More importantly, it has been demonstrated that in myocardial cells, desialylation of cells by neuraminidase treatment causes aberrant electrical activity (50), and may lead to arrhythmia (51).

In conclusion, we have generated the first mouse model of DMRV/h-IBM, which resembles the clinical, pathological and biochemical features of the disease in humans. The $Gne^{(-/-)}$h*GNE*V572L-Tg mouse is a concrete evidence that mutations in the *GNE* are causative of DMRV/h-IBM. Indeed, these DMRV/h-IBM mice will be a valuable tool to search for further clues in unraveling the pathomechanism of this myopathy. As we have clearly documented in these mice, hyposialylation plays a key role in the pathogenesis of DMRV/h-IBM, and is of paramount importance in considering therapeutic trials.

MATERIALS AND METHODS

Generation of *Gne* knockout mice

The *Gne* knockout mice [$Gne^{(-/-)}$] was produced in inGenious Targeting Laboratory (New York, NY, USA). The 17 kb mouse genomic DNA fragment, containing exons 3–5, was cloned from the mouse 129Sv/Ev lambda genomic library. The Neo cassette that was inserted replaced the 1.4 kb upstream of exon 3, exon 3 and 124 bp downstream of exon 3 (Fig. 1). The resulting targeting vector was linearized by *Not*I, purified and then transfected by electroporation into ES cells. Positive clones after neomycin selection were identified using PCR (primer sequences available upon request).

Generation of h*GNE*V572L-Tg

The cDNA for *GNE* mutant was obtained by reverse transcribed-PCR from skeletal muscle RNA of a DMRV patient with the V572L mutation and cloned into pCR-Blunt vector (Invitrogen, Carlsbad, CA, USA), as described previously (17). Cloned cDNA was sequenced by ABI cycle-sequencing procedures using an ABI 3100 (Applied Biosystems, Foster City, CA, USA). The *Xho*I fragment containing *GNE* mutant cDNA was excised and inserted into pCAGGS vector in which gene expression is driven by a CAG promoter (52). *loxP* sequences were introduced to flank the cDNA insert. *Sal*I fragment was purified and injected into C57BL/6 oocytes and subsequently transplanted into recipient mice. Founders were bred to WT C57BL/6 females to check for germline transmission, which was confirmed by PCR analyses on genomic DNA.

Production of $Gne^{(-/-)}$h*GNE*V572L-Tg

To maintain the same copy number of transgene, stringent measures were taken in generating mice. The h*GNE*V572L-Tg mouse was crossbred to *Gne* heterozygous mouse [$Gne^{(+/-)}$] to create a $Gne^{(+/-)}$ mouse that carried the human *GNE* [$Gne^{(+/-)}$h*GNE*V572L-Tg]. The latter was then mated with a $Gne^{(+/-)}$ mouse, to obtain a mouse that harbors the human V572L mutated *GNE* in a *Gne* knockout background.

For genotyping, DNA was isolated from mouse tails. *Gne* mice genotyping was carried out using PCR analysis on tail genomic DNA with the following primers: Neo, WT3 and S2 (primer sequences available upon request). Further, DNA was digested with *Bam*HI, subjected to Southern blotting and then analyzed by hybridization to a 500 bp probe.

For transgenic mice, the following oligonucleotides were used to amplify a 318 bp segment found specifically in human *GNE*: 1186F, CTTCAAGAGCCACTGCAAA; 1504R, CAATTCCTTCCCGAGGATT.

mRNA expression and determination of copy number

Mouse skeletal muscles, heart, brain, spleen and liver were dissected and rapidly frozen in liquid-nitrogen. Total RNA was extracted from cryostat sections of tissues with TRIzol (Invitrogen) following the manufacturer's protocol. First-strand cDNA was synthesized from RNA by reverse transcription using the Superscript RNase H^- Reverse Transcriptase (Invitrogen) and random hexamers. Gene expression was measured by quantitative real-time PCR in i-Cycler IQ system (Bio-Rad Laboratories, Hercules, CA, USA). Primers (1186F and 1504R) were used to span exon–intron junctions to prevent amplification of genomic DNA. Relative quantification of gene expression was determined by comparison of threshold values as suggested by the manufacturer. All results were normalized with respect to Gapdh expression.

Transgene copy number was determined by the i-Cycler IQ system using the SYBR Green reagent kit according to the manufacturer's instructions. Triplicate samples of tail DNA from transgenic mice of each line were analyzed concurrently against a standard curve of scaled concentrations of an external standard. Primers were designed to amplify the transgene h*GNE*V572L and endogenous *Gne*; twice the ratio of the h*GNE*V572L/*Gne* amplicons was interpreted as copy number.

Sialic acid measurement

The bound sialic acids from the serum and pieces of different tissues were released using 20 mM sulfuric acid hydrolysis for 1 h at 80°C. Free sialic acids were then derivitized with 1, 2-diamino-4, 5-methylenedioxybenzene and analyzed by reverse-phase HPLC fluorescence detection as described previously (53). The eluant was monitored by fluorescence and

Table 1. Antibodies used in the study

Antibody	Manufacturer	Type	Dilution
AβPP (6E10)	Chemicon International Inc., Temecula, CA, USA	Mouse monoclonal	1:1000
Aβ 1–40	Chemicon	Rabbit polyclonal	1:100
Aβ 1–42	Chemicon	Rabbit polyclonal	1:100
Aβ oligomer (A11)	Chemicon	Rabbit polyclonal	1:1000
Human beta site APP cleaving enzyme	Alpha Diagnostic International	Rabbit polyclonal	1:100
Caveolin 3	Transduction Laboratories, Lexington, KY, USA	Rabbit polyclonal	1:400
α-dystroglycan (VIA4-1)	Upstate Cell Signaling Solutions, Lake Placid, NY, USA	Mouse monoclonal	1:100
β-dystroglycan	A gift from Dr Ejiro Ozawa	Rabbit polyclonal	1:200
Grp94 (9G10)	Stressgen Biotechnologies, Calgary, Canada	Rat monoclonal	1:30
LAMP-1 (25)	BD Transduction Laboratories, Lexington, KY, USA	Mouse monoclonal	1:100
LAMP-2A	A gift from Dr Fumitaka Oyama	Rabbit polyclonal	1:100
LC3	A gift from Dr Tamotsu Yoshimori	Rabbit polyclonal	1:200
NCAM (123C3)	Santa Cruz Biotechnology Inc.	Mouse monoclonal	1:100
α-sarcoglycan (Ad1/20A6)	Novocastra Laboratories Ltd.	Mouse monoclonal	1:100
β-sarcoglycan (βSarc/5B1)	Novocastra Laboratories Ltd.	Mouse monoclonal	1:100
polyUbiquitin (FK1)	Biomol International	Mouse monoclonal	1:500
Neurofilament (SM-31)	Sternberg Monoclonals Inc., MD, USA	Mouse monoclonal	1:1000
Neurofilament (SM-310)	Sternberg Monoclonals Inc., MD, USA	Mouse monoclonal	1:1000
tau C	A gift from Dr Fumitaka Oyama	Rabbit polyclonal	1:1000

measured by comparison with Neu5Ac and Neu5Gc standards (from 0.05 nmol/μl to 5 nmol/μl). Total protein from tissues was measured using the Bio-Rad Protein Assay (Bio-Rad Laboratories) according to the manufacturer's protocol.

General assessment for motor strength and fatigability

Whole-animal strength and fatigability were measured according to a test procedure (here referred to as rod-climbing test) previously reported (54). In brief, this test required the mice to pull themselves on top of a suspended rod (3 mm in diameter). The measurement of muscle weakness was based on the mean percentage of passes over 15 trials of the test in a 3-min period. Fatigability was assessed as the average pass rate over time for each group of mice. The test was repeated at least three times after a 2-week period.

Histopathological and histochemical analyses

Fresh specimens from individual skeletal and cardiac muscles were snap-frozen in liquid-nitrogen-cooled isopentane and stored at −80°C until further processing. We stained frozen sections (6 μm) of transversal skeletal and cardiac muscles with a battery of histochemical stains including hematoxylin and eosin, modified Gomori trichrome and acid phosphatase. Sections were analyzed by light microscopy. We performed Congo red staining in 10 μm cryosections following the Putchler's modification, and viewed sections under light microscope and conventional fluorescence microscope using Texas-red filters (39). For immunohistochemical analysis, tissue sections were fixed either in acetone or paraformaldehyde, depending on the primary antibody used, and blocked with 5% normal serum and 2% bovine serum albumin in phosphate-buffered saline. The primary antibodies used are listed in Table 1. We used several antibodies which recognize amyloidβ. 6E10, which is a human-specific antibody, but also reacts to murine tissue when the amyloid burden is high, primarily recognizes AβPP (residues 1–16) after α-secretase cleavage. It also recognizes, in addition, C99 fragment and amyloid β peptides (1–40 and 1–42) which have been shown to be prone to aggregation. The anti-oligomeric antibody (A11) is specific to the oligomeric structure of β amyloid peptides. The following secondary antibodies were used appropriately: anti-goat IgG F (ab′)-2-fragment, FITC conjugated (EY Laboratories, San Mateo, CA, USA); anti-rabbit IgG (H + L), Alexa Fluor conjugated (Molecular Probes, Eugene, OR, USA); anti-mouse IgG1, FITC conjugated (Sanbio/Monosan, Uden, The Netherlands). Images were collected and analyzed with a laser scanning microscope (Olympus, Tokyo, Japan) with its appropriate software.

Morphometric analysis of fibers

Muscle cross sections were stained with rabbit polyclonal antibody against caveolin-3 followed by a fluorescent secondary antibody. Digital images from fluorescence signals were observed under a confocal microscope and the widest diameter was recorded for 600 or more fibers using Image-J software from the public domain NIH Image program (developed at the U.S. National Institutes of Health and available on the Internet at http://rsb.info.nih.gov/nih-image/). Results were analyzed using Statistics Software for Social Sciences (SPSS for Windows, Rel. 11.0.0. 2001, SPSS Inc., Chicago) software.

Electron microscopy

The muscle specimens were immediately fixed for 2 h in 2.5% cold glutaraldehyde with 0.1 M cacodylate buffer, pH 7.3. After washing in cacodylate buffer, the specimens were post-fixed in 1% osmium tetroxide in the same buffer, dehydrated with graded series of ethanol and embedded in Epon. Semithin sections (0.5 μm) were stained with toluidine blue alkaline. Ultrathin sections were stained with uranyl acetate, citrated and observed with a H-600 electron microscope (Hitachi, Tokyo, Japan) at 75 kV.

Serum CK

Blood samples were obtained either by inferior vena cava aspiration, or careful collection from mouse tail. Total CK activity was measured by a spectrophotometric assay employing a commercial kit (CPK-L Determiner, Kyowa MEDEX, Tokyo, Japan). For confirmation, CK isoforms were electrophoretically analyzed using Titan Gel CK Isozyme kit (Helena Laboratories, Beaumont, TX, USA) following the manufacturer's protocol.

Statistical analysis

Data were entered in SPSS version 11.0 and were analyzed by computation of the frequency and the mean ± SD and/or percentage. The data were then subjected to a univariate analysis (Fisher's exact test), Student's *t*-test, Wilcoxon paired test, ANOVA or Mann–Whitney *U* test, log-rank test or multiple regression analysis, whichever was appropriate. *P*-values less than 0.05 were considered to be statistically significant.

ACKNOWLEDGEMENTS

The authors thank the following persons for their invaluable support and assistance: Yoko Keira, Genri Kawahara, Mari Okada and Kumiko Murayama. This study is supported by the 'Research on Psychiatric and Neurological Diseases and Mental Health' from Health and Labour Sciences Research Grants; the 'Research on Health Sciences focusing on Drug Innovation' from the Japanese Health Sciences Foundation; the 'Research Grant (16B-2, 17A-10) for Nervous and Mental Disorders' from the Ministry of Health, Labour and Welfare; and the Program for Promotion of Fundamental Studies in Health Sciences of the National Institute of Biomedical Innovation (NIBIO).

Conflict of Interest statement. None declared.

REFERENCES

1. Nonaka, I., Sunohara, N., Ishiura, S. and Satoyoshi, E. (1981) Familial distal myopathy with rimmed vacuole and lamellar (myeloid) body formation. *J. Neurol. Sci.*, **51**, 141–155.
2. Argov, Z. and Yarom, R. (1984) 'Rimmed vacuole myopathy' sparing the quadriceps. A unique disorder in Iranian Jews. *J. Neurol. Sci.*, **64**, 33–43.
3. Nonaka, I., Noguchi, S. and Nishino, I. (2005) Distal myopathy with rimmed vacuoles and hereditary inclusion body myopathy. *Curr. Neurol. Neurosci. Rep.*, **5**, 61–65.
4. Ikeuchi, T., Asaka, T., Saito, M., Tanaka, H., Higuchi, S., Tanaka, K., Saida, K., Uyama, E., Mizusawa, H., Fukuhara, N. *et al.* (1997) Gene locus for autosomal recessive distal myopathy with rimmed vacuoles maps to chromosome 9. *Ann. Neurol.*, **41**, 432–437.
5. Mitrani-Rosenbaum, S., Argov, Z., Blumenfeld, A., Seidman, C.E. and Seidman, J.G. (1996) Hereditary inclusion body myopathy maps to chromosome 9p1-q1. *Hum. Mol. Genet.*, **5**, 159–163.
6. Nishino, I., Noguchi, S., Murayama, K., Driss, A., Sugie, K., Oya, Y., Nagata, T., Chida, K., Takahashi, T., Takusa, Y. *et al.* (2002) Distal myopathy with rimmed vacuoles is allelic to hereditary inclusion body myopathy. *Neurology*, **59**, 1689–1693.
7. Eisenberg, I., Avidan, N., Potikha, T., Hochner, H., Chen, M., Olender, T., Barash, M., Shemesh, M., Sadeh, M., Grabov-Nardini, G. *et al.* (2001) The UDP-*N*-acetylglucosamine 2-epimerase/*N*-acetylmannosamine kinase gene is mutated in recessive hereditary inclusion body myopathy. *Nat. Genet.*, **29**, 83–87.
8. Keppler, T., Hinderlich, S., Langner, J., Scwartz-Albiez, R., Reutter, W. and Pawlita, M. (1999) UDP-GlcNAc 2-epimerase: a regulator of cell surface sialylation. *Science*, **284**, 1372–1376.
9. Eisenberg, I., Grabov-Nardini, G., Hochner, H., Korner, M., Sadeh, M., Bertorini, T., Bushby, K., Castellan, C., Felice, K., Mendell, J. *et al.* (2003) Mutations spectrum of *GNE* in hereditary inclusion body myopathy sparing the quadriceps. *Hum. Mutat.*, **21**, 99.
10. Argov, Z., Eisenberg, I., Grabov-Nardini, G., Sadeh, M., Wirguin, I., Soffer, D. and Mitrani-Rosenbaum, S. (2003) Hereditary inclusion body myopathy: the Middle Eastern genetic cluster. *Neurology*, **60**, 1519–1523.
11. Tomimitsu, H., Shimizu, J., Ishikawa, K., Ohkoshi, N., Kanazawa, I. and Mizusawa, H. (2004) Distal myopathy with rimmed vacuoles (DMRV): new *GNE* mutations and splice variant. *Neurology*, **62**, 1607–1610.
12. Kim, B.J., Ki, C.S., Kim, J.W., Sung, D.H., Choi, Y.C. and Kim, S.H. (2006) Mutation analysis of the *GNE* gene in Korean patients with distal myopathy with rimmed vacuoles. *J. Hum. Genet.*, **51**, 137–140.
13. Ro, L.S., Lee-Chen, G.J., Wu, Y.R., Lee, M., Hsu, P.Y. and Chen, C.M. (2005) Phenotypic variability in a Chinese family with rimmed vacuolar distal myopathy. *J. Neurol. Neurosurg. Psychiatry*, **76**, 752–755.
14. Broccolini, A., Ricci, E., Cassandrini, D., Gliubizzi, C., Bruno, C., Tonoli, E., Silvestri, G., Pescatori, M., Rodolico, C., Sinicropi, S. *et al.* (2004) Novel *GNE* mutations in Italian families with autosomal recessive hereditary inclusion-body myopathy. *Hum. Mutat.*, **23**, 632.
15. Liewluck, T., Pho-Iam, T., Limwongse, C., Thongnoppakhun, W., Boonyapisit, K., Raksadawan, N., Murayama, K., Hayashi, Y.K., Nishino, I. and Sangruchi, T. (2006) Mutation analysis of the *GNE* gene in distal myopathy with rimmed vacuoles (DMRV) patients in Thailand. *Muscle Nerve*, Epub ahead of print.
16. Amouri, R., Driss, A., Murayama, K., Kefi, M., Nishino, I. and Hentati, F. (2005) Allelic heterogeneity of *GNE* gene mutation in two Tunisian families with autosomal recessive inclusion body myopathy. *Neuromuscul. Disord.*, **15**, 361–363.
17. Noguchi, S., Keira, Y., Murayama, K., Ogawa, M., Fujita, M., Kawahara, G., Oya, Y., Imazawa, M., Goto, Y., Hayashi, *et al.* (2004) Reduction of UDP-*N*-acetylglucosamine 2-epimerase/*N*-acetylmannosamine kinase activity and sialylation in distal myopathy with rimmed vacuoles. *J. Biol. Chem.*, **279**, 11402–11407.
18. Salama, I., Hinderlich, S., Shlomai, Z., Eisenberg, I., Krause, S., Yarema, K., Argov, Z., Lochmuller, H., Reutter, W., Dabby, R. *et al.* (2005) No overall hyposialylation in hereditary inclusion body myopathy myoblasts carrying the homozygous M712T GNE mutation. *Biochem. Biophys. Res. Commun.*, **328**, 221–226.
19. Hinderlich, S., Salama, I., Eisenberg, I., Potikha, T., Mantey, L.R., Yarema, K.J., Horstkorte, R., Argov, Z., Sadeh, M., Reutter, W. *et al.* (2004) The homozygous M712T mutation of UDP-*N*-acetylglucosamine 2-epimerase/*N*-acetylmannosamine kinase results in reduced enzyme activities but not in altered overall cellular sialylation in hereditary inclusion body myopathy. *FEBS Lett.*, **566**, 105–109.
20. Schwarzkopf, M., Knobeloch, K.P., Rohde, E., Hinderlich, S., Wiechens, N., Lucka, L., Horak, I., Reutter, W. and Horstkorte, R. (2002) Sialylation is essential for early development in mice. *Proc. Natl Acad. Sci. USA*, **99**, 5267–5270.
21. Mirabella, M., Alvarez, R.B., Bilak, M., Engel, W.K. and Askanas, V. (1996) Difference in expression of phosphorylated tau epitopes between sporadic and hereditary inclusion-body myopathies. *J. Neuropathol. Exp. Neurol.*, **55**, 774–786.
22. Akanas, V. and Engel, W.K. (2006) Inclusion-body myositis: a myodegenerative conformational disorder associated with Abeta, protein misfolding, and proteasome inhibition. *Neurology*, **66** (Suppl. 1), S39–S48.
23. Askanas, V. and Engel, W.K. (2003) Hereditary inclusion myopathies. In Rosenberg, R.N., Prusiner, S.B., DiMauro, S., Barchi, R.L. and Nestler, E.J. (eds), *The Molecular and Genetic Basis of Neurologic and Psychiatric Disease*, 3rd edn. Butterworth–Heinemann, Woburn, MA, USA, pp. 501–509.
24. Akanas, V. and Engel, W.K. (2003) Proposed pathogenic cascade of inclusion-body myositis: importance of amyloid-beta, misfolded proteins, predisposing genes, and aging. *Curr. Opin. Rheumatol.*, **15**, 734–744.
25. Horstkorte, R., Nöhring, S., Wiechens, N., Schwarzkopf, M., Danker, K., Reutter, W. and Lucka, L. (1999) Tissue expression and amino acid sequence of murine UDP-*N*-acetylglucosamine-2-epimerase/*N*-acetylmannosamine kinase. *FEBS J.*, **260**, 923–927.

26. Ishii, A., Hagiwara, Y., Saito, Y., Yamamoto, K., Yuasa, K., Sato, Y., Arahata, K., Shoji, S., Nonaka, I., Saito, I., Nabeshima, Y., Takeda, S. (1999) Effective adenovirus-mediated gene expression in adult murine skeletal muscle. *Muscle Nerve*, **22**, 592–599.
27. Kimpara, T., Imamura, T., Tsuda, T., Sato, K. and Tsuburaya, K. (1993) Distal myopathy with rimmed vacuoles and sudden death—report of two siblings. *Rinsho Shinkeigaku*, **33**, 886–890.
28. Nishino, I., Malicdan, M.C., Murayama, K., Nonaka, I., Hayashi, Y.K. and Noguchi, S. (2005) Molecular pathomechanism of distal myopathy with rimmed vacuoles. *Acta Myol.*, **24**, 80–83.
29. Sugarman, M., Kitazawa, M., Baker, M., Caiozzo, V.J., Querfurth, H.W. and LaFerla, F.M. (2006) Pathogenic accumulation of APP in fast twitch muscle of IBM patients and a transgenic model. *Neurobiol. Aging*, **27**, 423–432.
30. Post, J.A. (1992) Removal of sarcolemmal sialic acid residues results in a loss of sarcolemmal functioning and integrity. *Am. J. Physiol.*, **263**, H147–H152.
31. Bennett, E., Urcan, M.S., Tinkle, S.S., Kozkowski, A. and Levinson, S. (1997) Contribution of sialic acid to the voltage dependence of sodium channel gating: a possible electrostatic mechanism. *J. Gen. Physiol.*, **109**, 327–343.
32. Nishino, I. (2003) Autophagic vacuolar myopathies. *Curr. Neurol. Neurosci. Rep.*, **3**, 64–69.
33. Askanas, V., Alvarez, R.B. and Engel, W.K. (1993) β-Amyloid precursor epitopes in muscle fibers of inclusion body myositis. *Ann. Neurol.*, **34**, 551–560.
34. Askanas, V. and Engel, W.K. (1995) New advances in the understanding of sporadic inclusion-body myositis and hereditary inclusion-body myopathies. *Curr. Opin. Rheumatol.*, **7**, 486–496.
35. Ellis, R. and Pinheiro, T.J.T. (2002) Danger: misfolding proteins. *Nature*, **416**, 483–484.
36. Brooks, S.A., Dwek, M.V. and Schumacher, U. (2002) *Functional and Molecular Gycobiology*. BIOS Scientific Publishers Limited, Oxford, UK.
37. Helenius, A. and Aebi, M. (2004) Roles of *N*-linked glycans in the endoplasmic reticulum. *Annu. Rev. Biochem.*, **73**, 1019–1049.
38. Kumamoto, T., Fujimoto, S., Nagao, S., Masuda, T., Sugihara, R., Ueyama, H. and Tsuda, T. (1998) Proteasomes in distal myopathy with rimmed vacuoles. *Intern. Med.*, **37**, 746–752.
39. Askanas, V., Engel, W.K. and Alvarez, R.B. (1993) Enhanced detection of congo-red-positive amyloid deposits in muscle fibers of inclusion body myositis and brain of Alzheimer's disease using fluorescence technique. *Neurology*, **43**, 1265–1267.
40. Gregori, L., Hainfeld, J.F., Simon, M.N. and Goldbager, D. (1997) Binding of amyloid β protein to the 20S proteasome. *J. Biol. Chem.*, **272**, 58–62.
41. Wang, Y.P., Wang, X.C., Tian, Q., Yang, Y., Zhang, Q., Zhang, J.Y., Zhang, Y.C., Wang, Z.F., Wang, Q., Li, H. *et al.* (2006) Endogenous overproduction of β-amyloid induces tau hyperphosphorylation and decreases the solubility of tau in N2a cells. *J. Neural. Transm.*, Epub ahead of print.
42. McFarlane, I., Georgopoulou, N., Coughlan, C.M., Gillian, A.M. and Breen, K.C. (1999) The role of the protein glycosylation state in the control of cellular transport of the amyloid beta precursor protein. *Neuroscience*, **90**, 15–25.
43. Pahlsson, P. and Spitalnik, S.L. (1996) The role of glycosylation in synthesis and secretion of beta-amyloid precursor protein by Chinese hamster ovary cells. *Arch. Biochem. Biophys.*, **331**, 177–186.
44. Yazaki, M., Tagawa, K., Maruyama, K., Sorimachi, H., Tsuchiya, T., Ishiura, S. and Suzuki, K. (1996) Mutation of potential *N*-linked glycosylation sites in Alzheimer's disease amyloid precursor protein (APP). *Neurosci. Lett.*, **221**, 57–60.
45. Nakagawa, K., Kitazume, S., Oka, R., Maruyama, K., Saido, T.C., Sato, Y., Endo, T. and Hashimoto, Y. (2006) Sialylation enhances the secretion of neurotoxic amyloid-beta peptides. *J. Neurochem.*, **96**, 924–933.
46. Georgopoulou, N., McLaughlin, M., McFarlane, I. and Breen, K.C. (2001) The role of post-translational modification in beta-amyloid precursor protein processing. *Biochem. Soc. Symp.*, **67**, 23–36.
47. Tsai, B., Ye, Y. and Rapoport, T.A. (2002) Retro-translocation of proteins from the endoplasmic reticulum into the cytosol. *Nat. Rev. Mol. Cell Biol.*, **3**, 246–255.
48. Soeiro, M.N., Silva-Filho, F.C. and Meirelles, M.N. (1994) The nature of anionic sites and the endocytic pathway in heart muscle cells. *J. Submicrosc. Cytol. Pathol.*, **26**, 121–130.
49. Marengo, F.D., Wang, S.Y., Wang, B. and Langer, G.A. (1998) Dependence of cardiac cell Ca^{2+} permeability on sialic acid-containing sarcolemmal gangliosides. *J. Mol. Cell Cardiol.*, **30**, 127–137.
50. Woods, W.T., Inamura, K. and James, T.R. (1982) Electrophysiological and electron microscopic correlations concerning the effects of neuraminidase on canine heart cells. *Circ. Res.*, **50**, 228–231.
51. Ufret-Vincenty, C.A., Baro, D.J. and Santana, L.F. (2001) Differential contribution of sialic acid to the function of repolarizing K^+ currents in ventricular myocytes. *Am. J. Physiol. Cell Physiol.*, **281**, C464–C474.
52. Niwa, H., Yamamura, K. and Miyazaki, J. (1991) Efficient selection for high-expression transfectants with a novel eukaryotic vector. *Gene*, **108**, 193–199.
53. Hara, S., Yamaguchi, M., Takemori, Y., Nakamura, M. and Ohkura, Y. (1986) Highly sensitive determination of *N*-acetyl- and *N*-glycolylneuraminic acids in human serum and urine and rat serum by reversed-phase liquid chromatography with fluorescence detection. *J. Chromatogr.*, **377**, 111–119.
54. Keppler, O.T., Hinderlich, S., Langner, J., Schwartz-Albiez, R., Reutter, W. and Pawlita, M. (1999) UDP-GlcNAc 2-epimerase: a regulator of cell surface sialylation. *Science*, **284**, 1372–1376.

ELSEVIER

Brain & Development 29 (2007) 112–116

BRAIN & DEVELOPMENT
Official Journal of the Japanese Society of Child Neurology

www.elsevier.com/locate/braindev

Case Report

Familial reducing body myopathy

Maki Ohsawa [a,*], Teerin Liewluck [b], Katuhisa Ogata [c], Takahiro Iizuka [d], Yukiko Hayashi [b], Ikuya Nonaka [a], Masayuki Sasaki [a], Ichizo Nishino [b]

[a] *Department of Child Neurology, National Center Hospital for Mental, Nervous and Muscular Disorders, National Center of Neurology and Psychiatry (NCNP), Kodaira, Tokyo 187-8551, Japan*
[b] *Department of Neuromuscular Research, National Institute of Neuroscience, NCNP, Kodaira, Tokyo 187-8502, Japan*
[c] *Department of Neurology, National Center Hospital for Mental, Nervous and Muscular Disorders, NCNP, Kodaira, Tokyo 187-8551, Japan*
[d] *Department of Neurology, Kitasato University School of Medicine, Sagamihara, Kanagawa 228-8555, Japan*

Received 16 November 2005; received in revised form 22 June 2006; accepted 26 June 2006

Abstract

Reducing body myopathy (RBM) is a rare pathologically defined myopathy characterized by the presence of inclusion bodies which are abnormally stained by menadione–nitroblue–tetrazolium. The clinical symptoms vary widely as to the age of onset, disease progression and severity. Among the many reported patients, there have been only three families with this disorder, showing a manifold of clinicopathological features in each family. We report a fourth family with RBM affecting a boy and his mother. The proband (boy) began to have difficulty putting on his trousers at age 10 years and difficulty arising from a chair at 11 years. His spine was rigid. His mother, on the other hand, noticed foot-drop at the age 29, but the clinical course was rapidly progressive, and she was wheelchair-bound at 34 years. Both patients had generalized muscle weakness and atrophy and with mild CK elevation. Muscle pathology was characterized by the presence of atrophic fibers with reducing bodies in some areas. As these patients demonstrate, clinical symptoms in RBM are very variable, even within the same family. There are no specific clinical characteristics distinctive to RBM, thus further studies are necessary to characterize this disorder both clinically and pathologically.

Keywords: Reducing body myopathy; Familial; Mother and Son; Rapidly progressive

1. Introduction

Reducing body myopathy (RBM) is a group of heterogeneous disorders characterized pathologically by the presence of inclusion bodies that reduce nitroblue tetrazolium (NBT) in the absence of menadione as a substrate in the α-glycerophosphate dehydrogenase reaction. In 1972, Brooke and Neville initially described two unrelated girls with a severe congenital myopathy with reducing bodies [1]. The clinical spectrum of this disease is wide, showing different age of onset, course and severity of disease [2–10]. Although most of the cases have been sporadic, there have been three families with this disorder. Here, we report the fourth family with RBM and discuss the clinical and pathologic findings.

2. Patients and muscle pathology

2.1. Case history

The proband is an 11-year-old boy, the second of three children of a Japanese father and Filipino mother. Both his brothers were healthy except that the younger one had a history of Hirschsprung disease. Pregnancy

* Corresponding author. Tel.: +81 42 341 2711; fax: +81 42 344 6745.
E-mail address: mohsawa@ncnp.go.jp (M. Ohsawa).

0387-7604/$ - see front matter © 2006 Elsevier B.V. All rights reserved.
doi:10.1016/j.braindev.2006.06.010

and delivery were uneventful and psychomotor development was normal. Until 9 years of age, he could run faster than his classmates. At the age of 10 years and 5 months, he began to have difficulty putting on his trousers. One month after the onset, he developed foot-drop and began to fall frequently. Two months later, he had difficulty getting up from a sitting position. He could no longer run as fast as when he was 10 years old.

On physical examination, he had generalized muscle atrophy and weakness, especially around the shoulder, hip and anterior compartment of the lower legs. There was winging of the scapulae. Muscle weakness was slightly more marked on the left than the right. His spine was rigid on anteflexion and he had a lumbar lordosis. He was able to walk on his toes but not on his heels. Gowers' sign was positive. Deep tendon reflexes were diminished. Facial and extra-ocular muscles were normal. There were no fasciculations, calf muscle hypertrophy or pes cavus.

Cardiorespiratory functions were normal. The serum creatine kinase (CK) level was 495 IU/l (normal range 51–197 IU/l). Muscle CT scans revealed generalized volume loss, especially in the hamstrings, and areas of low density in the paraspinal muscles (Fig. 1). Needle electromyogram showed mixed neurogenic and myogenic patterns in biceps brachii and tibialis anterior muscles. Nerve conduction velocities of the median and tibialis posterior nerves were normal. No mutations were found in the SMN gene for spinal muscular atrophy; FSHD was ruled out by Southern blot.

The proband's mother is 35 years old. She developed foot-drop on the left at age 29 and became wheelchair-bound 5 years after the onset. Her father is Spanish and her mother is of Filipino and Chinese descent. Clinical examination revealed moderate generalized muscle atrophy and weakness. She was able to sit without support. She could raise her right arm up to the horizontal, but she was unable to raise her legs and left upper limb, against gravity. The spine was not rigid. Deep tendon reflexes were hypoactive. Facial and extra-ocular muscles were spared. The remainder of the physical examination was normal. Serum CK was slightly increased to 477 IU/l.

2.2. Muscle pathology

Muscle biopsy was performed on the left biceps brachii in the proband at age 11. His mother had two biopsies: left biceps brachii muscle and the left quadriceps femoris muscle at age 31. Biopsy specimens were frozen in isopentane cooled in liquid nitrogen. Serial 10 μm cryostat sections were stained with various histochemical methods. For electron microscopy, the muscle specimens were fixed in 2.5% glutaraldehyde in 0.1 M cacodylate buffer; ultrathin sections were double stained with uranyl acetate and lead citrate.

In the proband, there were clusters of atrophic fibers of 5–25 μm in diameter in a few fascicles (Fig. 2a–f), frequently with enlarged nuclei. Non-atrophic fibers showed moderate variation in fiber size ranging from 60–95 μm in diameter. Only a few fibers had internal nuclei. Endomysial fibrous tissue was increased in the atrophic fascicles. Adipose tissue was not increased. On modified Gomori trichrome (mGT), cytoplasmic bodies were seen in scattered fibers. There were no nemaline bodies, rimmed vacuoles or ragged-red fibers. On ATPase, there was mild fiber type grouping.

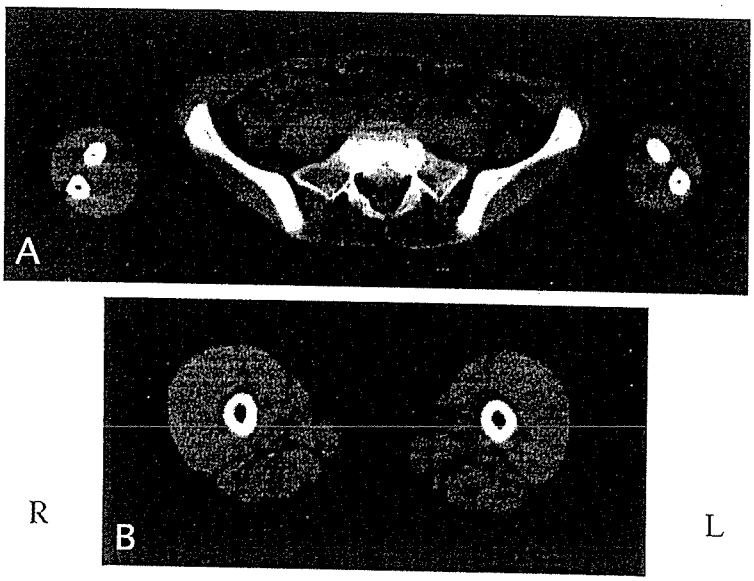

Fig. 1. Muscle computer tomography of the proband. The paraspinal muscles are almost totally replaced by fat tissue (A); the hamstring muscles are atrophic and exhibit moth-eaten appearance (B).

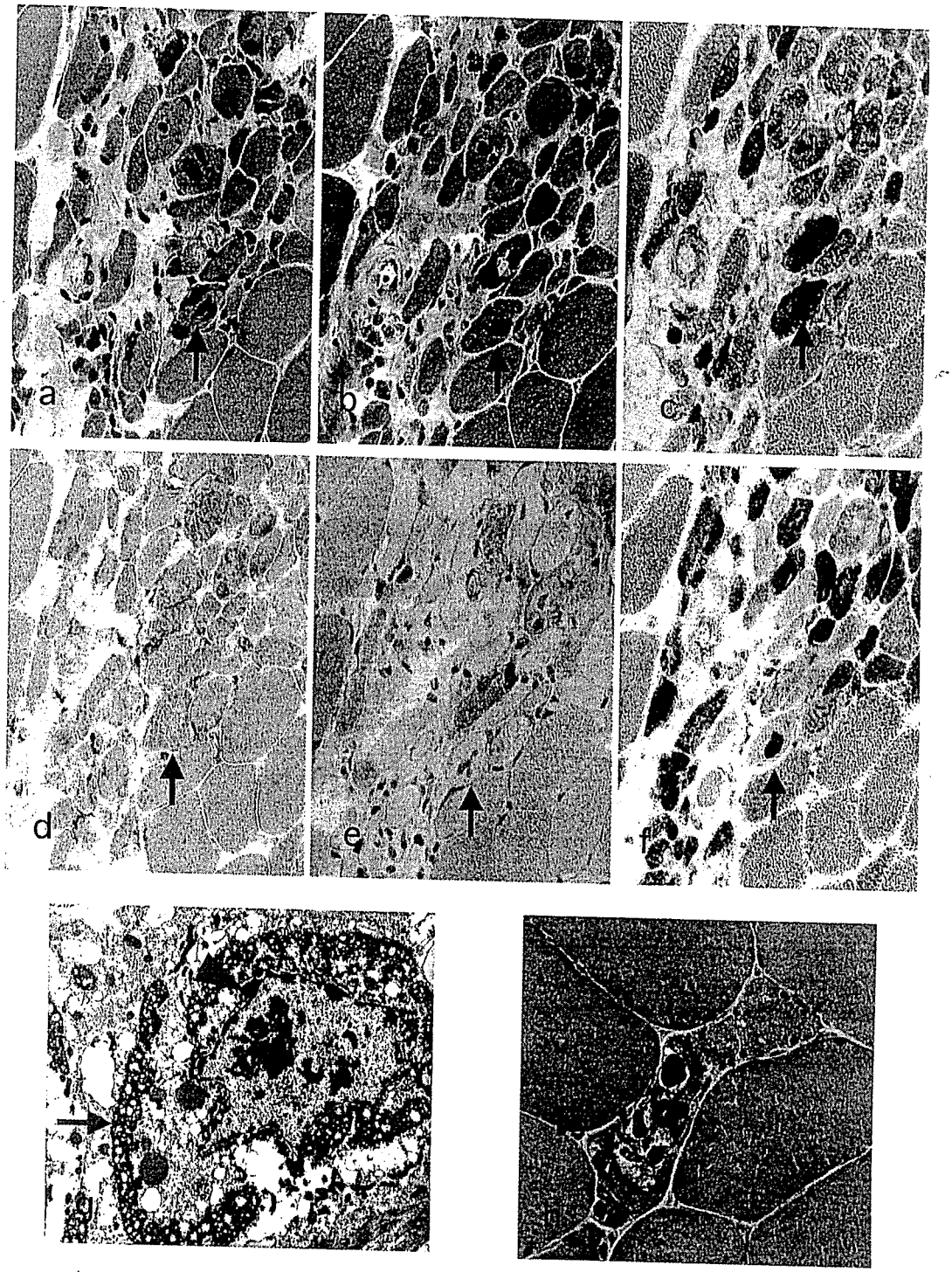

Fig. 2. Serial frozen sections (a–f) and an electron micrograph (g) from patient 1 and representative muscle pathology from patient 2 (h). In hematoxylin and eosin stain, atrophic fibers with reducing bodies are seen to be aggregated, (a). The reducing bodies are eosinophilic (a) and stained dark purple on modified Gomori trichrome (b), strongly reactive to NADH-TR (c), have increased enzymatic activity in acid phosphatase (d), and negative for periodic acid Schiff (PAS) staining suggesting that there is no glycogen component (e). They are strongly stained with MAG (f) showing "reducing activity" to nitroblue tetrazolium. Arrows in a–f indicate the same fiber with reducing bodies in serial sections. An electron micrograph of the reducing bodies (arrow) surrounding a degenerating nucleus (arrow head) suggesting a close relationship between nuclear change and inclusion body formation (g). In the proband's mother's muscle biopsy (h), there are fibers containing eosinophilic reducing bodies (arrow).

The most striking finding was the presence of reducing bodies in the atrophic fibers which were positively stained with both menadione-linked α-glycerophosphate dehydrogenase (MAG) and MAG without the substrate menadione. They were stained brilliant red with hematoxylin and eosin, dark purple with modified Gomori

trichrome, and dark blue with NADH-tetrazolium reductase.

On electron microscopy, these reducing bodies consisted of clusters of granular material with the same electron density as chromatin granules (Fig. 2g). They frequently encircled both normal-looking and degenerated myonuclei.

In the proband's mother, the overall pathological changes were similar although more fascicles were involved and contained very abundant reducing bodies (Fig. 2h). The inclusions were predominantly seen in type 1 fibers.

3. Discussion

Brooke and Neville were the first to describe two girls with congenital myopathy who had progressive and fatal courses [1] whose muscle biopsies were characterized by the presence of intracytoplasmic inclusion bodies. Since these inclusions reduce nitro-blue-tetrazolium (NBT) without a substrate in the α-glycerophosphate dehydrogenase reaction, the term "reducing body" was coined. Thereafter, many patients with reducing bodies in muscle biopsy have been reported as "reducing body myopathy" [2–10]. The onset of the disease varied from early childhood to adulthood, with different clinical symptoms; some had rapidly progressive and fatal course [1,6] and others showed a relatively benign course [2,5,9]. Initially, RBM was thought to be one of the congenital myopathies, although there is no characteristic clinical picture.

Although both our patients had proximal dominant muscle weakness and tibial muscle involvement other features varied: the onset of the disease was different, only the proband had rigid spine, and his mother's progression was quite rapid. Histopathologically, in both patients, some fascicles were preferentially affected. Inclusion bodies were seen mainly in the atrophic fibers.

There have been four families with RBM including the present family (Table 1) [2,7,10]. The modes of inheritance seem to be different from family to family: probable autosomal dominant or X-linked recessive inheritance in this family and in previous reports [7,8]. Hubner's family probably had an autosomal recessive inheritance. In familial RBM, many patients noticed their symptoms during school age, as in our proband; however, one patient developed weakness of the legs and hands after age 50 [10]. Rigid spine seems to be common in familial patients [7,10], but is not necessarily an initial sign and neither is it pathognomonic. Most patients had predominantly proximal muscle weakness and had no facial muscle involvement or pseudohypertrophy. Furthermore, serum CK was usually normal or only mildly elevated. However, there are no definite differences in clinical features between familial and spo-

Table 1
Previous reports of familial reducing body myopathy

Case	Sex	Onset age	Muscle weakness	Other symptoms	CK	Clinical course	Pathological findings	RB
Hubner et al. [2]	F	11	+	Respiratory insufficiency		27y: bed-ridden	Fibrosis	+
Sister	F	9	+	Respiratory insufficiency		15y: alive	Fibrosis	+
Reichmann et al. [7]	M	6	Proximal dominant	Rigid spine kyphosis	343	42y: wheelchair-bound, dead	Variation in fiber size fibrosis	+
Daughter	F	?	None	Rigid spine kyphosis				
Goebel et al. [10]	M	7	Proximal dominant	Rigid spine	174	8y: wheelchair-bound	Variation in fiber size	Many
Grand mother	F	50	Lower limbs dominant			70y: walk slowly	Small groups of atrophic fibers	+
Patient 1	M	10	Proximal dominant	Rigid spine	495	11y: unable to stand up without support	Focal atrophy	In atrophic fibers
Patient 2 (mother)	F	29	Proximal dominant		477	34y: wheelchair- bound	Focal atrophy	Mainly in atrophic fibers

CK: creatine kinase, RB: reducing body; ?: unknown.

radic patients. Pathologically, Goebel et al. [10] also reported that muscle fascicles with numerous inclusion bodies were adjacent to completely normal fascicles, and such focal degeneration seems to be a characteristic feature of this disorder [6]. It is still uncertain whether familial cases of RBM share a common pathogenetic mechanism with that in sporadic RBM.

Histopathologically there was fiber type grouping in our proband, suggesting a neurogenic process as well. Although needle electromyogram of the right tibialis anterior muscle showed a few giant spikes, careful clinical examination and peripheral nerve conduction studies showed no neurogenic changes. A prominent finding in RBM is that the atrophic fibers with reducing bodies are frequently aggregated in some fascicles, sparing the rest of the fascicle [6,10]. With disease progression, the changes extend diffusely and consequently fibrotic tissue proliferation ensues [6]. This selectivity of fascicular involvement may differ from muscle to muscle, reflecting different degrees and clinical variability.

The origin and significance of the reducing bodies remain unknown. Since these inclusions are usually present around and in the vicinity of myonuclei, association with nuclear changes appears possible, more so since these bodies have the same electron density as that of chromatin granules. By immunohistochemical staining, however, these bodies have no nuclear component.

Acknowledgements

We thank Ms Fumie Uematsu for taking electron micrographs on muscle biopsies. The authors thank Dr. May Christine V. Malicdan for her critical comments on the manuscript. This work is supported in part by the "Research on Health Sciences focusing on Drug Innovation" and the "Research on Psychiatric and Neurological Diseases and Mental Health" from the Japanese Health Sciences Foundation; in part by the "Grant-in-Aid for Scientific Research" from the Japan Society for the Promotion of Science; and in part by the "Research Grant (17A-10) for Nervous and Mental Disorders" from the Ministry of Health, Labour and Welfare.

References

[1] Brooke MH, Neville HE. Reducing body myopathy. Neurology 1972;22:829–40.
[2] Hübner G, Pongratz D. Reducing body myopathy – ultrastructure and classification (author's transl). Virchows Arch A Pathol Anat Histol 1981;392:97–104.
[3] Oh SJ, Meyers GJ, Wilson Jr ER, Alexander CB. A benign form of reducing body myopathy. Muscle Nerve 1983;6:278–82.
[4] Carpenter S, Karpati G, Holland P. New observations in reducing body myopathy. Neurology 1985;35:818–27.
[5] Bertini E, Salviati G, Apollo F, Ricci E, Servidei S, Broccolini A, et al. Reducing body myopathy and desmin storage in skeletal muscle: morphological and biochemical findings. Acta Neuropathol (Berl) 1994;87:106–12.
[6] Kiyomoto BH, Murakami N, Kobayashi Y, Nihei K, Tanaka T, Takeshita K, et al. Fatal reducing body myopathy. Ultrastructural and immunohistochemical observations. J Neurol Sci 1995;128:58–65.
[7] Reichmann H, Goebel HH, Schneider C, Toyka KV. Familial mixed congenital myopathy with rigid spine phenotype. Muscle Nerve 1997;20:411–7.
[8] Goebel HH. Congenital myopathies with inclusion bodies : a brief review. Neuromuscul Disord 1998;8:162–8.
[9] Figarella-Branger D, Putzu GA, Bouvier-Labit C, Pouget J, Chateau D, Fardeau M, et al. Adult onset reducing body myopathy. Neuromuscul Disord 1999;9:580–6.
[10] Goebel HH, Halbig LE, Goldfarb L, Schober R, Albani M, Neuen-Jacob E, et al. Reducing body myopathy with cytoplasmic bodies and rigid spine syndrome : a mixed congenital myopathy. Neuropediatrics 2001;32:196–205.

ABSTRACT: Reducing-body myopathy (RBM) is a rare myopathy characterized by the presence of unique sarcoplasmic inclusions called reducing bodies (RBs). We characterized the aggresomal features of RBs that contained γ–tubulin, ubiquitin, and endoplasmic reticulum (ER) chaperones, together with a set of membrane proteins, in a family with hereditary RBM. Increased messenger ribonucleic acid and protein levels of a molecular chaperone, glucose-related protein 78, were also observed. These results suggest that the unfolded protein response caused by the accumulation of misfolded proteins in the endoplasmic reticulum plays an important role in the formation of RBs.

Muscle Nerve **35**: 322–326, 2007

UNFOLDED PROTEIN RESPONSE AND AGGRESOME FORMATION IN HEREDITARY REDUCING-BODY MYOPATHY

TEERIN LIEWLUCK, MD,[1] YUKIKO K. HAYASHI, MD, PhD,[1] MAKI OHSAWA, MD,[2] RUMI KUROKAWA, BS,[1] MASAKO FUJITA, BS,[1] SATORU NOGUCHI, PhD,[1] IKUYA NONAKA, MD, PhD,[1] and ICHIZO NISHINO, MD, PhD[1]

[1] Department of Neuromuscular Research, National Institute of Neuroscience, National Center of Neurology and Psychiatry, 4-1-1 Ogawa-Higashi, Kodaira, Tokyo 187-8502, Japan
[2] Department of Child Neurology, National Center Hospital for Mental, Nervous and Muscular Disorders, National Center of Neurology and Psychiatry, Tokyo, Japan

Accepted 26 September 2006

The endoplasmic reticulum (ER) is the site where newly synthesized secretory and membrane proteins are folded and assembled under a stringent quality-control system that prevents the development of aberrant conformers. The accumulation of misfolded/unfolded proteins in the ER leads to the unfolded protein response (UPR) that enhances folding capacity by transcriptional induction of ER chaperones and translationally represses protein synthesis. Misfolded proteins are removed from the ER by retrotranslocation to the cytosol and degradation by the ubiquitin–proteasome system.[9] If these misfolded proteins fail to fold correctly and are not degraded by the proteasome, they are transported in a microtubule-dependent manner to the perinuclear microtubule-organizing center together with ubiquitin, ER chaperones, and form cytoplasmic aggregates called aggresomes.[3] Aggresomes are usually surrounded by a cage of reorganized intermediate filaments and undergo autophagolysosomal degradation.[3] Postmitotic cells, such as neurons and myocytes, are particularly vulnerable to the detrimental effects of aggresome accumulation because they cannot reduce potentially toxic substances through cell division.[9]

Reducing-body myopathy (RBM) is a rare myopathy characterized pathologically by the presence of intracytoplasmic inclusion bodies strongly stained by menadione-linked α-glycerophosphate dehydrogenase (MAG) in the absence of substrate, α-glycerophosphate.[1] The term "reducing body (RB)" implies the reducing activity of the inclusions to nitroblue tetrazolium in the absence of substrate. This condition is also commonly associated with rimmed vacuoles and cytoplasmic bodies. The clinical features of RBM are variable and can be classified into three forms, namely (1) severe infantile form,[1,8] (2) benign congenital form,[13] and (3) late onset form.[2]

This article includes Supplementary Material available via the internet at http://www.mrw.interscience.wiley.com/suppmat/0148-639X/suppmat/

Abbreviations: endoplasmic reticulum stress-associated degradation; G3PDH, glyceraldehyde-3-phosphate dehydrogenase; GRP, glucose-regulated protein; ER, endoplasmic reticulum; hRBM, hereditary reducing body myopathy; IBMPFD, inclusion body myopathy associated with Paget's disease of bone and frontotemporal dementia; MAG, menadione-linked α-glycerophosphate dehydrogenase; mRNA, messenger ribonucleic acid; RB, reducing-body; RBM, reducing-body myopathy; RT-PCR, reverse transcriptase–polymerase chain reaction; sRBM, sporadic reducing-body myopathy; UPR, unfolded protein response; VCP, valosin-containing protein

Key words: aggresome; endoplasmic reticulum stress; endoplasmic reticulum stress-associated degradation (EDRA); reducing-body myopathy; unfolded protein response

Correspondence to: Y. K. Hayashi; e-mail: hayasi_y@ncnp.go.jp

Published online 10 November 2006 in Wiley InterScience (www.interscience.wiley.com). DOI 10.1002/mus.20691

Table 1. Results of immunoreaction of reducing body (RB) in the hereditary RB myopathy (hRBM) muscle.

Protein category	Immunoreactivity	
	Positive	Negative
Nucleoplasm	None	Nuclei, nucleoli
Nuclear envelope	Emerin, Lamin A, Lamin C, LAP2	Lamin B
Centrosome	γ-tubulin (C)	None
UPR	IRE1α, p-PERK, GRP78, GRP94, Calnexin, ERp72, PDI	None
ERAD	VCP, Polyubiquitin, 26S proteasome P27 subunit (P)	None
Cytoplasmic chaperones	HSP70	αB crystallin
Internal membranes	GM130, Limp1, LAMP2, SERCA1, SERCA2	None
Intermediate filaments	Desmin (P)	None
Sarcomere	Actin (P)	α-actinin, MHC fast, MHC slow, Titin, Telethonin
Plasma membrane	Dystrophin, α-, β-DG, α-SG, Dysferlin, Caveolin-3, nNOS, Integrin α7B, ILK, Paxillin,	None
Basal lamina and extracellular matrix	None	Merosin, Collagen VI
Others	Caspase-3, Polyglutamine	Neurofilament, Plectin, β amyloid 1-40, 1-42

UPR, unfolded protein response; ERAD, endoplasmic reticulum stress-associated degradation; C, central staining of RB; VCP, valosin-containing protein; P, peripheral staining of RB.

Most of the patients have sporadic disease and only a few familial cases have been reported.[4,7] Here we report the aggresomal features of RBs found in a new family with hereditary RBM (hRBM).

MATERIALS AND METHODS

Patients. Details of the clinical features of this family with hRBM have been described elsewhere.[11] Briefly, patient 1 is an 11-year-old boy of Japanese and Filipino descent in good health until 10 years of age, when he developed proximal-dominant muscle weakness and spinal rigidity. Serum creatine kinase was elevated to 495 IU/L (normal <70 IU/L), and a muscle biopsy was performed from the left biceps brachii at 11 years of age. Patient 2 is the mother of patient 1, a 35-year-old Filipino. She noticed asymmetrical generalized muscle weakness at 29 years of age and became wheelchair-bound 5 years later. No spinal rigidity was observed. Serum creatine kinase level was elevated to 417 IU/L, and muscle biopsy was performed at the age of 31 years.

Muscle specimens from both patients displayed scattered MAG-positive cytoplasmic inclusions in the absence of substrate, α-glycerophosphate. Some muscle fibers contained rimmed vacuoles. Atrophic fibers that partly clustered in groups and scattered cytoplasmic bodies were also seen in the specimen from patient 1. On electron microscopy, RBs frequently engulfed myonuclei and consisted of clusters of granular materials with electron density similar to chromatin.

Immunohistochemical and Western Blot Analyses. The antibodies used in this study are listed in the table which appears as supplementary material athttp://www.mrw.interscience.wiley.com/suppmat/0148-639X/suppmat/. Immunohistochemical and Western blot analyses were performed as previously described.[6] The sections were incubated overnight with primary antibodies at 4°C. Immunostaining was also performed using muscle specimens from two previously reported patients with a severe, sporadic infantile form of RBM (sRBM).[8]

Quantitative RT-PCR. Total ribonucleic acid was extracted from frozen muscles of patient 1, one sRBM, and three age-matched controls as previously described.[8] Quantitative reverse transcriptase–polymerase chain reaction (RT-PCR) was performed using iCycler (Bio-Rad Laboratories, Richmond, California) adhering to the manufacturer's protocol. Primer sequences for the 78-kDa glucose-regulated protein (*GRP78*) gene (F: 5′-GTGGTAGTGCAAGCTGAAGG; R: 5′-TGGAGTCTCACTCTTGTCGC) and glyceraldehyde-3-phosphate dehydrogenase (*G3PDH*) gene (F: 5′-GGTAAAGTGGATATTGTTGCCATCAATG; R: 5′-GGAGGGATCTCGCTCCTGGAAGATGGTG) were used. The values of GRP78 mRNA were normalized to that of G3PDH.

Mutation Analysis. Genomic deoxyribonucleic acid was isolated from peripheral lymphocytes using a standard technique. Sequence analysis of the valosin-containing protein (*VCP*) gene was directly performed using ABI PRISM 3100 automated sequencer (Applied Biosystems Japan, Tokyo, Japan). Informazhy;eb;n;jtion on primer sequence and condi-

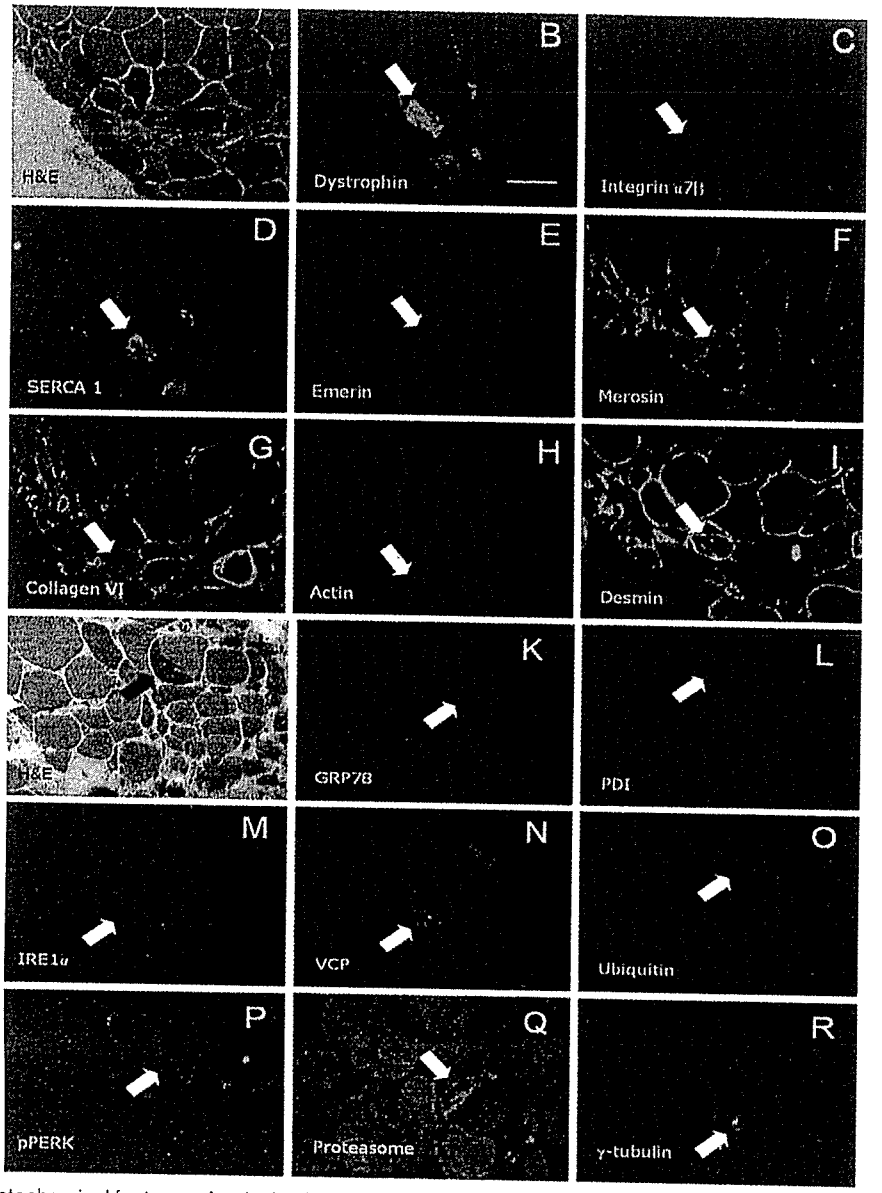

FIGURE 1. Immunohistochemical features of reducing bodies (RBs, arrows) in patient 1. **(A–I)** and **(J–R)** are serial sections. RBs appears as brightly eosinophilic sarcoplasmic inclusion on hematoxylin and eosin **(A,J)**. Various plasma membrane proteins such as dystrophin **(B)** and integrin α7B **(C)** as well as internal membrane protein SERCA1 **(D)** and nuclear membrane protein, emerin **(E)** are present in RBs. No immunoreactivity for extracellular matrix proteins including merosin **(F)** and collagen VI **(G)** is seen. Actin **(H)** and desmin **(I)** occasionally form a cage encircling RBs. RBs are also highlighted by antibodies against unfolded protein response-related molecules such as GRP78 **(K)**, PDI **(L)**, and IRE1α **(M)**, as well as ERAD-related proteins including VCP **(N)** and polyubiquitin **(O)**. Immunoreactivity of p-PERK **(P)**, an active form of PERK, confirms the activation of unfolded protein response. Proteasome **(Q)** stains only the periphery of reducing body while γ-tubulin **(R)** predominantly marks its center. Scale bar, 40 μm.

tions of polymerase chain reaction are available upon request.

RESULTS

Immunohistochemical and Western Blot Analyses. RBs were strongly stained for the various antibodies used in the muscles from hRBM (Table 1, Fig. 1). Serial sections revealed that larger-sized RBs showed positive immunoreactions for polyubiquitin, ER chaperones, membrane-associated proteins, nuclear envelope proteins, and caspase-3. The periphery of the RBs was immunoreactive for the proteasome P27 subunit, actin, and desmin, and the center of the RBs was immunoreactive for γ-tubulin, a centrosome-specific tubulin. Immunoblotting analysis revealed an increased amount of

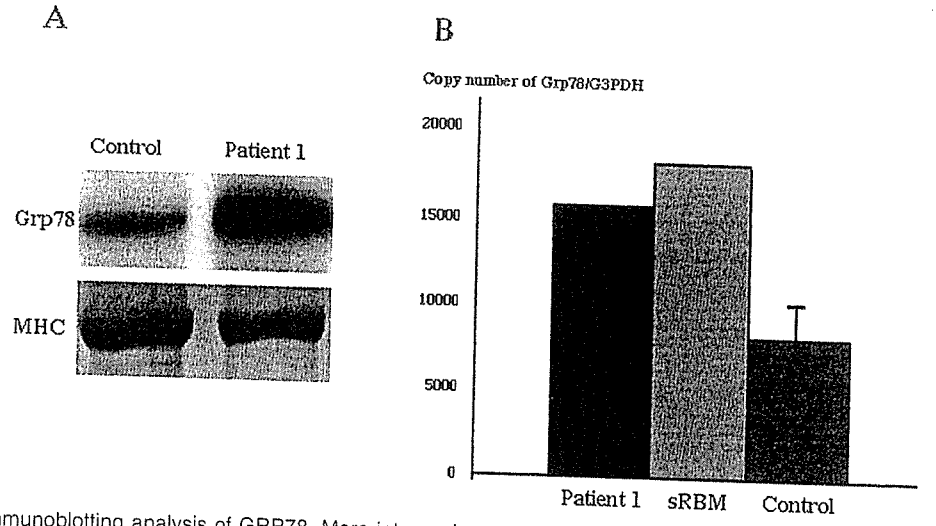

FIGURE 2. (A) Immunoblotting analysis of GRP78. More intense immunoreactive band for GRP78 is seen in patient 1. MHC: myosin heavy chain. (B) Histogram represents the results of quantitative RT-PCR for GRP78 on muscle biopsies. GRP78 in patient 1 and a sporadic reducing-body myopathy (sRBM) patient is upregulated compared to the control samples.

GRP78 expression in muscle from patient 1 compared to the control muscle (Fig. 2A).

Quantitative RT-PCR. The expression of GRP78 mRNA was much higher in the muscles from both patient 1 and one sRBM than the control muscles (Fig. 2B).

Mutation Analysis. No mutation was identified in the *VCP* gene in either patient 1 or 2.

DISCUSSION

Recently, aggresomal features of the inclusion bodies have been reported in several neurodegenerative disorders including Huntington's and Parkinson's diseases. Inclusions observed in Huntington's disease are specifically composed of mutant huntingtin together with ER chaperones and ubiquitin, whereas α-synuclein is the major component in Lewy bodies observed in Parkinson's disease.[9]

In this study, we demonstrated that RBs observed in hRBM patients contained virtually all membrane-associated proteins examined including those of nuclei, sarcoplasmic reticulum, Golgi apparatus, lysosome, and plasma membrane. RBs also had aggresomal features; i.e., positive immunoreaction for ubiquitin and ER chaperones, and positive central immunoreaction for γ-tubulin, and were surrounded by desmin, a major intermediate filament protein of skeletal muscle. Furthermore, increased mRNA and protein levels of GRP78 were observed in the muscle from the hRBM patient. GRP78 is a molecular chaperone, which is upregulated during UPR. Positive immunoreaction for phosphorylated (activated) pancreatic ER kinase observed in RBs also indicates the activation of UPR. From these results, accumulation of various misfolded membrane proteins in ER could be a primary event in hRBM patients, which results in activation of the UPR and subsequent aggresome formation. γ-Tubulin is a marker of the centrosome. Although postmitotic cells like muscle fibers and neurons normally do not contain a centrosome, γ-tubulin distinctly exists in the cytosol. In neurons, the cytosolic γ-tubulins could be reorganized to form juxtanuclear condensation under ER stress, and this lesion could be the microtubule organization center.[9] Positive immunoreaction for γ-tubulin in the center of RBs also suggests ER stress in hRBM.

Except for the consistency of ubiquitin immunoreactivity, previous reports showed equivocal immunohistochemical results of RBs.[2] To know whether the present results could apply to other patients with RBM, we also examined muscle specimens from two sRBM patients with the severe infantile form of the disease. All RBs found in sRBM patients yielded positive immunoreactivity of GRP78, ubiquitin, and emerin, but only a subset of RBs was highlighted by dystrophin and α-sarcoglycan. A desmin-positive rim was not seen in RBs in the sRBM muscles. Deposition of the proteins associated with UPR and ER-associated degradation, together with upregulation of GRP78 mRNA also indicates the activation of UPR in sRBM muscle samples.

Recently, a mutation in the *VCP* gene, a key molecule in the retrotranslocation step of ER stress-associated degradation, was identified in patients with inclusion-body myopathy associated with Paget's disease of bone and frontotemporal dementia (IBMPFD).[14] Due to the similarity of VCP-positive inclusions observed in the hRBM to that in IBMPFD, sequence analysis of the *VCP* gene was performed. However, no mutation was identified in the patients with hRBM.

In conclusion, our data show the aggresomal features of RBs, which might be induced by accumulation of a battery of membrane-associated proteins, resulting in the activation of UPR. To determine the precise pathomechanism of RBM, detailed analyses on the functions of ER chaperones and proteasomes should be investigated. In animal studies, overexpression of chaperones or application of chaperone-inducing compounds such as radicicol is beneficial for the treatment of neurodegenerative diseases with inclusion bodies.[9] Upregulation of chaperone transcription may be an option for the development of therapy in RBM.

We thank Dr. A. Kakizuka (Kyoto University, Japan) for providing the antibody for VCP, and Dr. M. Astejada (National Institute of Neuroscience, Tokyo, Japan) for reviewing the article. This work was supported by the Research on Health Sciences focusing on Drug Innovation from the Japanese Health Sciences Foundation; by the Research on Psychiatric and Neurological Diseases and Mental Health of Health and Labor Sciences research grants and the research grant (17A-10) for nervous and mental disorders from the Ministry of Health, Labor and Welfare; by a Grant-in-Aid for Scientific Research from the Japan Society for the Promotion of Science; and by the Program for Promotion of Fundamental Studies in Health Sciences of the National Institute of Biomedical Innovation.

REFERENCES

1. Brooke MH, Neville HE. Reducing body myopathy. Neurology 1972;22:829–840.
2. Figarella-Branger D, Putzu GA, Bouvier-Labit C, Pouget J, Chateau D, Fardeau M, et al. Adult onset reducing body myopathy. Neuromuscul Disord 1999;9:580–586.
3. Garcia-Mata R, Gao YS, Sztul E. Hassles with taking out the garbage: aggravating aggresomes. Traffic 2002;3:388–396.
4. Goebel HH, Halbig LE, Goldfarb L, Schober R, Albani M, Neuen-Jacob E, et al. Reducing body myopathy with cytoplasmic bodies and rigid spine syndrome: a mixed congenital myopathy. Neuropediatrics 2001;32:196–205.
5. Hayashi YK, Chou FL, Engvall E, Ogawa M, Matsuda C, Hirabayashi S, et al. Mutations in the integrin alpha7 gene cause congenital myopathy. Nat Genet 1998;19:94–97.
6. Hayashi YK, Ogawa M, Tagawa K, Noguchi S, Ishihara T, Nonaka I, et al. Selective deficiency of alpha-dystroglycan in Fukuyama-type congenital muscular dystrophy. Neurology 2001;57:115–121.
7. Hubner G, Pongratz D. Reducing body myopathy—ultrastructure and classification. Virchows Arch A Pathol Anat Histol 1981;392:97–104.
8. Kiyomoto BH, Murakami N, Kobayashi Y, Nihei K, Tanaka T, Takeshita K, et al. Fatal reducing body myopathy. Ultrastructural and immunohistochemical observations. J Neurol Sci 1995;128:58–65.
9. Muchowski PJ, Wacker JL. Modulation of neurodegeneration by molecular chaperones. Nat Rev Neurosci 2005;6:11–22.
10. Noguchi M, Takata T, Kimura Y, Manno A, Murakami K, Koike M, et al. ATPase activity of p97/valosin-containing protein is regulated by oxidative modification of the evolutionally conserved cysteine 522 residue in Walker A motif. J Biol Chem 2005;280:41332–41341.
11. Ohsawa M, Liewluck T, Ogata K, Iizukad T, Hayashi Y, Nonaka I, et al. Familial reducing body myopathy. Brain Dev (in press).
12. Sakaki M, Koike H, Takahashi N, Sasagawa N, Tomioka S, Arahata K, et al. Interaction between emerin and nuclear lamins. J Biochem (Tokyo) 2001;129:321–327.
13. Tome FM, Fardeau M. Congenital myopathy with "reducing bodies" in muscle fibres. Acta Neuropathol (Berl) 1975;31:207–217.
14. Watts GD, Wymer J, Kovach MJ, Mehta SG, Mumm S, Darvish D, et al. Inclusion body myopathy associated with Paget disease of bone and frontotemporal dementia is caused by mutant valosin-containing protein. Nat Genet 2004;36:377–381.